EUROPEAN ORGANISATION FOR NUCLEAR RESEARCH

CERN-PPE/91-189
7 November, 1991

Properties of Multihadronic Events with a Final State Photon at $\sqrt{s} = M_{Z^0}$

The OPAL Collaboration

Abstract

The properties of final state photons in multihadronic decays of the Z^0 and those of the recoiling hadronic system are discussed and compared with theoretical expectations. The yield of two and three jet events with final state photons is found to be in good agreement with the expectation from a matrix element calculation of $O(\alpha\alpha_s)$. Uncertainties in the interpretation of the theoretical calculation do not yet permit a final assessment of events with just one reconstructed jet. Comparing the rates of two jet events with a photon to those of three jet events in the inclusive multihadronic sample, the strong coupling constant in second order is determined as $\alpha_s(M_{Z^0}) = 0.122 \pm 0.010$, taking into account only the statistical and experimental systematic errors. It is found that an abelian model of the strong interaction does not describe the data. The comparison of the total yield and the jet rates with QCD shower programs shows better agreement with the ARIADNE model than with the JETSET model. Both programs are found to describe well the photon properties and the properties of the residual hadronic event.

(Submitted to Zeitschrift für Physik)

The OPAL Collaboration

P.D. Acton[25], G. Alexander[23], J. Allison[16], P.P. Allport[5], K.J. Anderson[9], S. Arcelli[2], P. Ashton[16], A. Astbury[a], D. Axen[b], G. Azuelos[18,c], G.A. Bahan[16], J.T.M. Baines[16], A.H. Ball[17], J. Banks[16], G.J. Barker[13], R.J. Barlow[16], J.R. Batley[5], G. Beaudoin[18], A. Beck[23], J. Becker[10], T. Behnke[27], K.W. Bell[20], G. Bella[23], P. Berlich[10], S. Bethke[11], O. Biebel[3], U. Binder[10], I.J. Bloodworth[1], P. Bock[11], B. Boden[3], H.M. Bosch[11], S. Bougerolle[b], B.B. Brabson[12], H. Breuker[8], R.M. Brown[20], R. Brun[8], A. Buijs[8], H.J. Burckhart[8], P. Capiluppi[2], R.K. Carnegie[6], A.A. Carter[13], J.R. Carter[5], C.Y. Chang[17], D.G. Charlton[8], P.E.L. Clarke[25], I. Cohen[23], W.J. Collins[5], J.E. Conboy[15], M. Cooper[22], M. Couch[1], M. Coupland[14], M. Cuffiani[2], S. Dado[22], G.M. Dallavalle[2], S. De Jong[8], P. Debu[21], L.A. del Pozo[5], M.M. Deninno[2], A. Dieckmann[11], M. Dittmar[4], M.S. Dixit[7], E. Duchovni[26], G. Duckeck[11], I.P. Duerdoth[16], D.J.P. Dumas[6], G. Eckerlin[11], P.A. Elcombe[5], P.G. Estabrooks[6], E. Etzion[23], F. Fabbri[2], M. Fincke-Keeler[a], H.M. Fischer[3], D.G. Fong[17], C. Fukunaga[24], A. Gaidot[21], O. Ganel[26], J.W. Gary[4], J. Gascon[18], R.F. McGowan[16], N.I. Geddes[20], C. Geich-Gimbel[3], S.W. Gensler[9], F.X. Gentit[21], G. Giacomelli[2], V. Gibson[5], W.R. Gibson[13], J.D. Gillies[20], J. Goldberg[22], M.J. Goodrick[5], W. Gorn[4], C. Grandi[2], F.C. Grant[5], J. Hagemann[27], G.G. Hanson[12], M. Hansroul[8], C.K. Hargrove[7], P.F. Harrison[13], J. Hart[5], P.M. Hattersley[1], M. Hauschild[8], C.M. Hawkes[8], E. Heflin[4], R.J. Hemingway[6], R.D. Heuer[8], J.C. Hill[5], S.J. Hillier[1], D.A. Hinshaw[18], C. Ho[4], J.D. Hobbs[8], P.R. Hobson[25], D. Hochman[26], B. Holl[8], R.J. Homer[1], A.K. Honma[e], S.R. Hou[17], C.P. Howarth[15], R.E. Hughes-Jones[16], R. Humbert[10], P. Igo-Kemenes[11], H. Ihssen[11], D.C. Imrie[25], A.C. Janissen[6], A. Jawahery[17], P.W. Jeffreys[20], H. Jeremie[18], M. Jimack[2], M. Jobes[1], R.W.L. Jones[13], P. Jovanovic[1], D. Karlen[6], K. Kawagoe[24], T. Kawamoto[24], R.K. Keeler[a], R.G. Kellogg[17], B.W. Kennedy[15], C. Kleinwort[8], D.E. Klem[19], T. Kobayashi[24], T.P. Kokott[3], S. Komamiya[24], L. Köpke[8], J.F. Kral[8], R. Kowalewski[6], H. Kreutzmann[3], J. von Krogh[11], J. Kroll[9], M. Kuwano[24], P. Kyberd[13], G.D. Lafferty[16], F. Lamarche[18], W.J. Larson[4], J.G. Layter[4], P. Le Du[21], P. Leblanc[18], A.M. Lee[17], M.H. Lehto[15], D. Lellouch[26], P. Lennert[11], C. Leroy[18], J. Letts[4], S. Levegrün[3], L. Levinson[26], S.L. Lloyd[13], F.K. Loebinger[16], J.M. Lorah[17], B. Lorazo[18], M.J. Losty[7], X.C. Lou[12], J. Ludwig[10], M. Mannelli[8], S. Marcellini[2], G. Maringer[3], A.J. Martin[13], J.P. Martin[18], T. Mashimo[24], P. Mättig[3], U. Maur[3], J. McKenna[a], T.J. McMahon[1], J.R. McNutt[25], F. Meijers[8], D. Menszner[11], F.S. Merritt[9], H. Mes[7], A. Michelini[8], R.P. Middleton[20], G. Mikenberg[26], J. Mildenberger[6], D.J. Miller[15], R. Mir[12], W. Mohr[10], C. Moisan[18], A. Montanari[2], T. Mori[24], M.W. Moss[16], T. Mouthuy[12], B. Nellen[3], H.H. Nguyen[9], M. Nozaki[24], S.W. O'Neale[8,d], B.P. O'Neill[4], F.G. Oakham[7], F. Odorici[2], M. Ogg[6], H.O. Ogren[12], H. Oh[4], C.J. Oram[e], M.J. Oreglia[9], S. Orito[24], J.P. Pansart[21], B. Panzer-Steindel[8], P. Paschievici[26], G.N. Patrick[20], S.J. Pawley[16], P. Pfister[10], J.E. Pilcher[9], J.L. Pinfold[26], D. Pitman[a], D.E. Plane[8], P. Poffenberger[a], B. Poli[2], A. Pouladdej[6], E. Prebys[8], T.W. Pritchard[13], H. Przysiezniak[18], G. Quast[27], M.W. Redmond[9], D.L. Rees[1], K. Riles[4], S.A. Robins[13], D. Robinson[8], A. Rollnik[3], J.M. Roney[9], E. Ros[8], S. Rossberg[10], A.M. Rossi[2,f], M. Rosvick[a], P. Routenburg[6], K. Runge[10], O. Runolfsson[8], D.R. Rust[12], S. Sanghera[6], M. Sasaki[24], A.D. Schaile[10], O. Schaile[10], W. Schappert[6], P. Scharff-Hansen[8], P. Schenk[a], H. von der Schmitt[11], S. Schreiber[3], J. Schwiening[3], W.G. Scott[20], M. Settles[12], B.C. Shen[4], P. Sherwood[15], R. Shypit[b], A. Simon[3], P. Singh[13], G.P. Siroli[2], A. Skuja[17], A.M. Smith[8], T.J. Smith[8], G.A. Snow[17], R. Sobie[g], R.W. Springer[17], M. Sproston[20], K. Stephens[16], H.E. Stier[10,†], R. Ströhmer[11], D. Strom[9], H. Takeda[24], T. Takeshita[24], P. Taras[18], S. Tarem[26], P. Teixeira-Dias[11], N.J. Thackray[1], G. Transtromer[25], T. Tsukamoto[24], M.F. Turner[5], G. Tysarczyk-Niemeyer[11], D. Van den plas[18],

R. Van Kooten[8], G.J. VanDalen[4], G. Vasseur[21], C.J. Virtue[19], A. Wagner[27], C. Wahl[10], J.P. Walker[1], C.P. Ward[5], D.R. Ward[5], P.M. Watkins[1], A.T. Watson[1], N.K. Watson[8], M. Weber[11], P. Weber[6], S. Weisz[8], P.S. Wells[8], N. Wermes[11], M. Weymann[8], M.A. Whalley[1], G.W. Wilson[21], J.A. Wilson[1], I. Wingerter[8], V-H. Winterer[10], N.C. Wood[16], S. Wotton[8], T.R. Wyatt[16], R. Yaari[26], Y. Yang[4,h], G. Yekutieli[26], M. Yurko[18], I. Zacharov[8], W. Zeuner[8], G.T. Zorn[17].

[1]School of Physics and Space Research, University of Birmingham, Birmingham, B15 2TT, UK
[2]Dipartimento di Fisica dell' Università di Bologna and INFN, Bologna, 40126, Italy
[3]Physikalisches Institut, Universität Bonn, D-5300 Bonn 1, FRG
[4]Department of Physics, University of California, Riverside, CA 92521 USA
[5]Cavendish Laboratory, Cambridge, CB3 0HE, UK
[6]Carleton University, Dept of Physics, Colonel By Drive, Ottawa, Ontario K1S 5B6, Canada
[7]Centre for Research in Particle Physics, Carleton University, Ottawa, Ontario K1S 5B6, Canada
[8]CERN, European Organisation for Particle Physics, 1211 Geneva 23, Switzerland
[9]Enrico Fermi Institute and Department of Physics, University of Chicago, Chicago Illinois 60637, USA
[10]Fakultät für Physik, Albert Ludwigs Universität, D-7800 Freiburg, FRG
[11]Physikalisches Institut, Universität Heidelberg, Heidelberg, FRG
[12]Indiana University, Dept of Physics, Swain Hall West 117, Bloomington, Indiana 47405, USA
[13]Queen Mary and Westfield College, University of London, London, E1 4NS, UK
[14]Birkbeck College, London, WC1E 7HV, UK
[15]University College London, London, WC1E 6BT, UK
[16]Department of Physics, Schuster Laboratory, The University, Manchester, M13 9PL, UK
[17]Department of Physics and Astronomy, University of Maryland, College Park, Maryland 20742, USA
[18]Laboratoire de Physique Nucléaire, Université de Montréal, Montréal, Quebec, H3C 3J7, Canada
[19]National Research Council of Canada, Herzberg Institute of Astrophysics, Ottawa, Ontario K1A 0R6, Canada
[20]Rutherford Appleton Laboratory, Chilton, Didcot, Oxfordshire, OX11 0QX, UK
[21]DPhPE, CEN Saclay, F-91191 Gif-sur-Yvette, France
[22]Department of Physics, Technion-Israel Institute of Technology, Haifa 32000, Israel
[23]Department of Physics and Astronomy, Tel Aviv University, Tel Aviv 69978, Israel
[24]International Centre for Elementary Particle Physics and Dept of Physics, University of Tokyo, Tokyo 113, and Kobe University, Kobe 657, Japan
[25]Brunel University, Uxbridge, Middlesex, UB8 3PH UK
[26]Nuclear Physics Department, Weizmann Institute of Science, Rehovot, 76100, Israel
[27]Universität Hamburg/DESY, II Inst. für Experimental Physik, 2000 Hamburg 52, FRG

[a]University of Victoria, Dept of Physics, P O Box 3055, Victoria BC V8W 3P6, Canada
[b]University of British Columbia, Dept of Physics, 6224 Agriculture Road, Vancouver BC V6T 1Z1, Canada
[c]Also at TRIUMF, Vancouver, Canada V6T 2A3

[d]On leave from Birmingham University, Birmingham B15 2TT, UK
[e]Univ of Victoria, Dept of Physics, P.O. Box 1700, Victoria BC V8W 2Y2, Canada and TRIUMF, Vancouver, Canada V6T 2A3
[f]Present address: Dipartimento di Fisica, Università della Calabria and INFN, 87036 Rende, Italy
[g]University of British Columbia, Dept of Physics, 6224 Agriculture Road, Vancouver BC V6T 2A6, Canada and IPP, McGill University, High Energy Physics Department, 3600 University Str, Montreal, Quebec H3A 2T8, Canada
[h]On leave from Research Institute for Computer Peripherals, Hangzhou, China
[†]deceased 25th March 1991

1 Introduction

Photons in multihadronic decays of the Z^0 [1, 2, 3, 4] may be used to probe fundamental properties of the Standard Model. Since the direct coupling of the Z^0 to the photon is forbidden, an anomalous rate of events containing photons could provide the first glimpse of a substructure of the Z^0 [5]. More conventionally, photons radiated from quarks (fig. 1) test the strength and structure of both the electroweak and strong sectors of the Standard Model. As suggested in [6] these photons, being messengers from the primary quarks, have been exploited to measure the weak coupling constants of up and down type quarks [2, 4]. In this paper we focus on QCD tests.

We report on the properties of final state photons in multihadronic Z^0 decays and on the topology of the recoiling hadronic system. We compare our measurements with a matrix element calculation of $O(\alpha\alpha_s)$ [7] and with predictions from two QCD shower models that include both photon and gluon radiation [8, 9]. Although these latter predictions are based on different concepts of the parton shower, they describe the general features of the inclusive multihadronic event sample succesfully over a wide range of centre-of-mass energies. Photons from final state radiation, being sensitive to the evolution of quarks in the parton branching, offer new and specific QCD tests. They provide means of disentangling the gluon contribution. Since, apart from the coupling strength the theoretical descriptions of photon and gluon emission from quarks are alike, there is little freedom to change the photon radiation once the gluon contributions are fixed.

The photon sample in this analysis is the same as that used for the measurement of the electroweak couplings of up and down type quarks in a previous publication [2], where the selection procedure, the background estimate, and the correction procedure are discussed in detail. Since the experimental procedure and the theoretical ambiguities are important for some of the physics topics analysed here, we will summarise in sections 2 to 5 the salient features of the analysis and provide some details on our experimental checks. Section 6 gives an overview of the theoretical predictions for final state photon production. Results are given in section 7. We present measurements of the total yield of events with final state photons. From the production cross sections for events with a photon and specific jet multiplicities we derive values for the strong coupling constant α_s and test the existence of the gluon self coupling, one of the cornerstones of QCD. Finally, we present measurements of several properties of the photon and the general event topology and compare them to the predictions of QCD shower models. Our conclusions are summarised in section 8.

2 The OPAL Detector

This analysis is based on an integrated luminosity of approximately 6.6 pb^{-1} collected with the OPAL detector [10] at LEP. The data were recorded at centre-of-mass energies E_{cm} between 88.28 and 94.28 GeV around the Z^0 pole.

The most important components of OPAL for this study are the tracking chambers and the barrel part of the electromagnetic calorimeter. The central detector provides a measurement

of the momenta of charged particles in a magnetic field over almost the entire solid angle. The electromagnetic calorimeter covers the solid angle in $|\cos\theta| \leq 0.98$, where θ is the polar angle with respect to the beam direction. The barrel part ($|\cos\theta| \leq 0.82$) consists of 9440 lead glass blocks of 24.6 radiation lengths, pointing towards the interaction region and each subtending an angular region of approximately 40x40 mrad^2. A presampler for electromagnetic showers and a hadron calorimeter offer cross checks of the photon identification. The barrel presampler is located between the magnet coil and the lead glass calorimeter. It consists of a set of 16 double-planed chambers containing streamer-tubes with both wire and cathode-strip readout. The barrel hadron calorimeter, consisting of nine planes of streamer-tube chambers within the iron return yoke of the magnet, is located directly behind the electromagnetic calorimeter. In addition to measuring hadron energies, it provides information on longitudinal shower development.

3 Selection of Events with Final State Photons

The final state photon sample is obtained in three steps: first a sample of multihadronic events is selected. As a second step we search for isolated clusters in the lead glass calorimeter with topological properties which are unlikely for neutral hadrons. Finally the detailed structure of these clusters is used to reject background of hadronic origin. Details are described in [2].

- Multihadronic events are selected essentially by requiring a minimum number of tracks and clusters in the lead glass calorimeter together with a large energy deposition. We keep 145,095 events.

- To suppress background from neutral hadronic particles we then search for clusters of more than 7.5 GeV with a polar angle of $|\cos\theta| < 0.72$. To reject the potential background due to neutral hadrons which are overwhelmingly accompanied by additional particles, we demand the photon candidate to be isolated. No additional cluster or track is allowed within a cone of half opening angle 15 degrees around the direction of the photon candidate.

  In order to be able to compare our measurements with the theoretical calculations we further require the photon to have a minimum invariant mass when combined with the jets in the hadronic system. We first group the hadrons into jets [11] such that the pair mass $y = M_{ij}^2/E_{vis}^2$ of two jets i, j is always larger than a predefined y_{cut}. Here $M_{ij}^2 = 2 \cdot E_i E_j (1 - \cos\alpha_{ij})$, E_i and E_j being the energies of the jets and α_{ij} their opening angle. The visible energy E_{vis} is the sum of the momenta of all tracks and the energies of the clusters in the event including the photon. Corrections for double counting [12] in the tracking chamber and in the lead glass calorimeter and for losses due to neutrinos and neutral hadrons have been applied.

  Events are retained if the minimum mass of all combinations of the photon candidate with the jets $min(M_{\gamma j}^2/E_{vis}^2)$ exceeds y_{cut}. We choose values of y_{cut} between 0.005 and 0.2. Detailed studies of the event properties are performed for y_{cut}=0.005 and 0.06 for which we keep 339 and 171 events, respectively.

- To further suppress hadronic background we reject clusters with properties not compatible with the expectation for genuine photons. We only accept clusters of less than 16 blocks,

a width calculated from the first moment of the cluster of less than 30 mrads, and a cluster shape, measured from the energy sharing of blocks, which is consistent with that of a photon.

After these cuts we retain 276 events for y_{cut}=0.005 and 149 events for y_{cut}=0.06.

4 Background Contributions to the Photon Sample

The background to the photon sample was determined from the data themselves and has been discussed in detail in [2]. We base our estimate on the number of isolated charged tracks which can be translated into the expected number of neutral hadrons using isospin symmetry. The dominant background is due to π^0's. From the number of isolated charged particles folded with the probability to reject π^0's with our cuts, we estimate their contribution to be 8.3±4.4 and 1.5±1.4 events for a y_{cut} of 0.005 and 0.06, respectively. Additional background is due to K^0_L's, neutrons or overlapping neutral particles like $K^{*0} \rightarrow K^0_L\pi^0$ or $K^0_s \rightarrow \pi^0\pi^0$. In general, these lead to much broader clusters than photons and are mostly rejected by our cuts. We estimate their contribution as 1.2±1.2 and 0.3±0.3 for the two y_{cut} values. Background from $\eta \rightarrow \gamma\gamma$ and $\omega^0 \rightarrow \gamma\pi^0$, which cannot be estimated with charged particles, is expected to be negligible from simulation studies.

Cross checks were made by fitting the cluster shape distribution [2] with a sum of photon and background contributions and by using the electromagnetic presampler which is sensitive to the different shower development of π^0's and photons in the coil and the hadron calorimeter to study the shower leakage. They lead to background estimates consistent with the above values.

Additional background to the final state photons is due to initial state photons. Taking their dependence on the centre-of-mass energy into account, we expect 13.3±1.3 (10.1±1.0) initial state photons for y_{cut} = 0.005 (0.06) using the Monte Carlo generator of [13].

5 Correction Procedure

To compare our measurements with theoretical predictions, we correct for biases introduced by the detector and the selection requirements using the JETSET simulation of the final state photon radiation [8]. The simulated events are passed through a detailed simulation of the OPAL detector [14]. For any distribution $f(x)$, we obtain the bin by bin correction factors $c(x) = n_{gen}(x)/n_{det}(x)$. Here n_{gen} denotes the number of generated events with a photon and n_{det} the number of events after simulating the detector and applying the experimental cuts. The bin size for the determination of $c(x)$ is chosen so that there are only small bin to bin migrations from the true x to the observed one. For all distributions the generated events are selected by applying y_{cut} to jets formed directly from the partons produced in the QCD shower.

We distinguish two kinds of corrections. The first, c_1, accounts for the effects of imposing energy and isolation cuts on the photon, but neglects distortions from the detector. For low

values of y, c_1 is substantial and depends on the proper description of photon radiation in the simulation. However, since $y \propto E_\gamma \cdot (1 - \cos\alpha)$ with α being the angle between the photon and a jet, we expect this correction to become less important for larger values of y. A second correction c_2 then accounts for the detector performance alone.

In fig. 2 we display typical efficiencies $\epsilon_1 = 1/c_1$ for photons produced with $|\cos\theta| < 0.72$, the polar angular range of our observed photons as predicted by JETSET and ARIADNE. In fig. 2a the efficiency is displayed as a function of y_{cut}. At low y_{cut} significant losses (52% at y_{cut}=0.005) are dominantly due to the energy cut. For $y_{cut} \geq 0.06$ losses are around 10% independent of y_{cut} and entirely due to the isolation requirement. The efficiency ϵ_1 is displayed in figs. 2b,and 2c as a function of the photon energy E_γ for y_{cut}=0.005 and 0.06. For the low y_{cut} the losses are about 25% for E_γ between 7.5 and 30 GeV. For $E_\gamma \rightarrow E_{beam}$ almost all events are accepted. The efficiency is significantly larger for y_{cut}=0.06, with a typical loss of 10%. The correction c_2 for the detector effects is typically 5-10% independent of y_{cut}. Note that a further correction of 43% for the restricted angular range of accepted photons has to be applied. In addition to the corrections for the topological cuts, the correction c_2 includes a contribution from the efficiency of the photon selection determined from a reference sample of $e^+e^- \rightarrow \gamma\gamma$ [15] and radiative lepton pair events. We lose 5.7±2.2% of the photons due to conversions before and in the tracking chambers and 5.0±1.6% due to the requirements on the cluster shape.

5.1 The Systematic Errors of the Corrections

We consider both the modelling of photon emission and the detector simulation as potential sources of systematic errors. As a first check of the quality of the simulation we compare the uncorrected spectra of the energy E_γ and the polar angle $|\cos\theta_\gamma|$ of the photon for data and Monte Carlo (figs. 3a,b). The predicted yield is normalised to the observed one. Significant errors in the modelling of the event structure or in the detector simulation should lead to discrepancies between data and model. The observed good agreement gives us confidence in the correction procedure.

In the following two sections we summarise which systematic errors we will consider for the event properties discussed in section 7 and how we estimate them. They apply to all distributions. Typical values for the size of the errors will be given for the yield.

5.1.1 Systematic Errors in the Modelling of Photon Emission

Since we cannot compare the predicted photon yield directly with the data for photon energies below 7.5 GeV and for isolation cones of smaller than 15 degrees, we have to rely on the simulation to correct for these losses. We assign a systematic uncertainty $\delta c_1(y_{cut})$ of 25% of the losses due to those requirements. For the total cross section this results in a systematic uncertainty of 13% at y_{cut}=0.005 and 4.5% for $y_{cut} \geq 0.04$. For some event distributions $f(x)$ this systematic error may depend on the value of x. For example for the efficiency in the photon energy for y_{cut}=0.005 as displayed in fig. 2b, we assign a systematic error of 6% at E_γ= 15 GeV and of 2.5% at E_γ= 40 GeV.

Various cross checks suggest that our error assignment is appropriate. As one cross check we compared the efficiencies obtained with the two Monte Carlo generators JETSET [8] and ARIADNE [9], which include final state photons. As can be seen in fig. 2 the efficiencies are similar, the largest difference being 5%. It should be noted that their predicted absolute photon yields differ by about 40%.

In addition we studied the potential bias on the observed photon yield due to the rather stringent isolation requirement. The estimate of these losses depends critically on the modelling of soft hadronisation. The energy and particle flow in multihadronic events has been analysed in much detail and found to be well described by simulations involving string fragmentation (see e.g. [16]). For our photon events we examined the particle flow just outside the isolation cone. The distribution of $(1/N)(dN/d\cos\alpha)$, α being the smallest angle per event of a track or a cluster with respect to the photon candidate, is shown in figs. 4a,b for $y_{cut} = 0.005$ and 0.06, respectively. The simulation agrees with the data. In a conservative approach we take the small (though not significant) excess of data in the first bin as an indication of a possible bias. Extrapolating the excess into the isolation cone, we estimate a potential systematic uncertainty of the yield of 2% and 3% for the two y_{cut} values. Secondly we changed the isolation requirement. By allowing a maximum energy in the isolation cone of 500 MeV instead of 0 MeV, and an isolation cone of 12.5 or 17.5 degrees we observe changes consistent with the assigned errors on the modelling of photon emission discussed above.

5.1.2 Systematic Uncertainties from the Detector Simulation

As discussed above, the photon detection efficiency has been determined with a reference sample of genuine photons. We use its statistical uncertainty as the systematic error of the photon detection efficiency for our analysis.

Another uncertainty stems from a potential misrepresentation of the measured direction and energy of the jets in the simulation. We estimate the quality of the reconstruction by using events with two jets and a photon according to the prescription of section 3. Since we assume the jets to be massless for these cross checks, we impose a small y_{cut}=0.02. To estimate the angular resolution of the jet direction we boost the hadronic part of the event into its rest system given by the photon momentum and

$$M_{recoil} = E_{cm}\sqrt{1 - 2 \cdot E_\gamma / E_{cm}}. \qquad (1)$$

In this system the two jets should be approximately collinear. The acolinearity angle between the sum of momenta of the two hemispheres is displayed in fig. 4c both for the data and for the simulation. The average value of 4.0±0.4 degrees in the data agrees well with the expectation of 4.2±0.2 degrees. The quality of the energy reconstruction is estimated by using the relation

$$E_i \;=\; E_{cm} \cdot \frac{\sin\alpha_{jl}}{\Sigma \sin\alpha_{mn}}, \qquad (2)$$

which is valid for three massless particles. Here E_i is the energy of the jet i and α_{jl} is the angle between the other jet and the photon. The sum goes over all three angles between jets and photon. This allows us to determine the jet energies rather independently of the energy

resolution of the detector. In fig. 4d we display

$$\frac{\delta E}{E} = \frac{E_{meas} - E_{recon}}{E_{meas}},$$

where E_{meas} is the jet energy as obtained from the sum of track and cluster energies, and E_{recon} is the energy obtained from relation (2). The data are well reproduced by the simulation. The data and Monte Carlo distributions are both centred near zero with average values of at -0.079±0.037 and -0.019 and widths of 0.24 and 0.23, respectively

We estimate the potential systematic uncertainty of the corrections due to the quality of the reconstruction by smearing the reconstructed energy and direction and by rescaling the jet energies. Changing the energy resolution by an additional 15%, or the angular resolution by 15 degrees has a negligible effect on the results. A rescaling of the jet energies by ±6%, to represent possible deviations as discussed in the previous paragraph, has small effects on the distributions (e.g. the yield changes by 2.7%) and is included in the systematic error.

In summary, several consistency checks with the data were made to estimate systematic errors. The largest one is due to uncertainties in the modelling of photon emission in phase space regions outside our selection, particularly important for low values of y_{cut}. In addition, we have to account for a potential systematic distortion of the jet energies. We will consider these two error sources for all distributions discussed in section 7.

6 Theoretical Predictions for Final State Radiation

Currently there are three theoretical predictions for final state photons in multihadronic events. Whereas the matrix element calculation of $O(\alpha\alpha_s)$ [7] is only available for the absolute yields of up to three partons and a photon, the parton shower models JETSET [8] and ARIADNE [9] predict in addition all event features and photon properties. Each is discussed below.

It should be noted that in all cases the electromagnetic coupling constant α has to be taken in the Thomson limit since we are dealing with real photons [17].

6.1 The Matrix Element Calculation

Kramer and Lampe have calculated the cross sections $\sigma_{\gamma+n\ jets}$ in $O(\alpha\alpha_s)$ for $n \leq 3$ as a function of y_{cut} [7]. This prediction has been derived from that of the jet rates for the inclusive hadronic event sample. Their result is expressed as

$$\sigma(Z^0 \rightarrow \gamma + \ jets)(y_{cut}) = \ \Sigma_{n=1}^{n=3}\sigma_n(y_{cut}) \qquad (3)$$

with the n-jet cross section σ_n

$$\sigma_1(y_{cut}) \propto b_1(y_{cut}) + \frac{\alpha_s}{2\pi} \cdot b_1'(y_{cut})$$

$$\sigma_2(y_{cut}) \propto b_2(y_{cut}) + \frac{\alpha_s}{2\pi} \cdot b_2'(y_{cut})$$

$$\sigma_3(y_{cut}) \propto \frac{\alpha_s}{2\pi} \cdot b_3(y_{cut})$$

The coefficients b_i and b_i' are given for discrete values of y_{cut} between 0.005 and 0.2. The primed coefficients contain the contributions from $O(\alpha_s)$ corrections. The value for σ_3 is a tree level result, σ_1 and σ_2 include complete corrections of $O(\alpha_s)$ [1]. It should be noted that since the jet rates are only given to first order in α_s, the result only depends on the *ratio* of $\Lambda_{\overline{MS}}$ and the renormalisation scale $\mu^2 = f \cdot E_{cm}^2$. Therefore no explicit variation of the scale will be considered. Both the absolute yield and the jet rates for events with final state photons depend on α_s.

The comparison of the matrix element calculation and the data is complicated by ambiguities in the definition of α_s and the jet definitions. These are both discussed below.

Assuming standard model electroweak quark couplings no free parameter appears in the theoretical prediction apart from α_s. The possible range of the predicted photon yield is therefore unambiguously given by the variation of α_s. As the calculation of [7] is first order in α_s, we adopt the value $\alpha_s^{(1)}$=0.177±0.013, which is the first order α_s value as obtained from the jet rates in the multihadronic Z^0 decays. This value agrees well with $\alpha_s^{(1)}$=0.161±0.012, as obtained from the ratio of two and three jet fractions in our final state photon event sample (see section 7.2.1). To include the uncertainty of the theoretical prediction due to the value of α_s we use as a upper bound 0.19, and as a lower bound α_s=0.118, which is the second order α_s value obtained from the jet rates in multihadronic Z^0 decays [18].

The ambiguities in the jet definition arise because we have to compare the theoretical expression for massless partons with the measurement of massive jets. It was shown for the analysis of jet rates in general multihadronic events [19], that the results of the calculations agree well with data if we adopt the jet finding algorithm of [11] corresponding to the 'E0' recombination scheme.

Another discrepancy between the matrix element calculation and our analysis stems from the different procedure for the event definition.

- For this analysis the relation between photon and jets was determined in two steps. At first only the hadrons were grouped into jets according to a certain y_{cut} value, and then the minimum jet-photon mass was calculated.
- Kramer and Lampe, dealing with at most three partons, *immediately* include the photon in the jet definition for some y_{cut} value. An event is discarded if a parton and a photon are combined into a new 'jet'.

In the absence of a matrix element for the differential distributions of the $q\bar{q}\gamma(g)$ events, we have estimated the corresponding distortions introduced by the different procedures by applying them separately to the $O(\alpha_s^2)$ matrix element for an abelian model of strong interactions as implemented in [8]. In this case we have selected only contributions from $q\bar{q}g$ and $q\bar{q}gg$ and

[1] The coefficients b_i of [7] are different from those used in [2]. In the meantime Kramer and Lampe have calculated the $O(\alpha_s)$ correction to the one jet rate and a reevaluation of the coefficients given to us previously showed that b_3 was too low by a factor 2. These changes do not affect the basic conclusions and values of the weak quark couplings given in [2].

replaced one gluon by a photon. We expect very close agreement between this model and the $q\bar{q}\gamma(g)$ distribution. As will be discussed in the next section, we find only small differences for the two event definitions at lower y_{cut} and large jet multiplicities but a significant difference for the one jet rate at large y_{cut} values.

6.2 Parton Shower Models

Apart from giving the absolute rates, the shower models [8, 9] offer predictions on the detailed properties of the photons and of the residual hadronic event structure. On the other hand they are based on an approximate treatment of QCD. In the two models JETSET and ARIADNE the jet development is simulated respectively by a parton or colour dipole cascade with subsequent hadronisation according to the string picture. Photon emission competes at each step of the cascade with gluon emission from either a quark or a gluon or gluon splitting into a quark pair. For example the differential probability for gluon (g) or photon (γ) emission, $q_1 \rightarrow q_2(g,\gamma)$, is approximately given by

$$\frac{dP}{dt} \propto \int_{z_{min}(t)}^{z_{max}(t)} dz[\frac{\alpha_s(Q^2)}{2\pi} P_{q_1 \rightarrow q_2,g}(z) + \frac{\alpha}{2\pi} P_{q_1 \rightarrow q_2,\gamma}(z)], \quad (4)$$

with t being an evolution parameter (see below), α_s, α_{em} the strong and electromagnetic coupling strength in leading order, and z the sharing of energy and momentum between q_2 and (γ, g). $P_{q_1 \rightarrow q_2,(g,\gamma)}$ is the Altarelli-Parisi splitting function [20] (modified in ARIADNE), which is identical for gluon and photon emission apart from factors for the colour or electromagnetic charge. In fact Sudakov form factors are also included for the branching probabilities used in the parton shower models. The integration limits z_{min}, z_{max} are defined in JETSET mainly by mass cutoffs, in ARIADNE by p_T cutoffs, where p_T is the transverse momentum with respect to the initial quark direction.

Ambiguities in these prescriptions and differences between these models are due to the various possible interpretations of variables like z, t, and the argument of α_s (for a discussion of some of these see [21]). In a given model the various parameter values are significantly constrained from the topology of multihadronic events which both programs, JETSET and ARIADNE, describe well for centre-of-mass energies between 14 and 91 GeV. The two models differ in some of these prescriptions, e.g. they require different QCD scale parameters: Λ_{JETSET} = 290 MeV, $\Lambda_{ARIADNE}$ = 200 MeV to describe the inclusive multihadronic event sample and use different evolution parameters $t_{JETSET} = \ln(m_{q_1}^2/\Lambda^2)$, $t_{ARIADNE} = \ln(p_T^2/\Lambda^2)$. In addition there are conceptual differences of the parton evolution once a gluon has been emitted. In JETSET the gluons and quarks branch, apart from kinematical constraints, independently from the rest of the event. In ARIADNE the emission of a gluon is due to colour dipoles between gluons and quarks, and the photon emission is due to electromagnetic dipoles between quarks. As a result, the emission affects the kinematics of both quarks. This implies that the models potentially predict different properties of events with final state photon radiation although both models reproduce the event shapes and particle distributions of the inclusive hadronic event sample very well. Final state photons are therefore a new probe of the basic mechanisms of parton evolution invoked in the two models.

The ambiguities mentioned above lead to uncertainties in the predictions of the shower models. For this analysis we adopt the default parametrisations with parameter values opti-

mised to describe the event shape distributions [22] for the whole multihadronic sample. Our analysis then tests whether photon and gluon emission can be described consistently. As the only uncertainty we consider the variation of the QCD scale parameter Λ (see discussion in [6]). Its possible range is taken from fits to the measured three jet rate [18] yielding ± 30 MeV for both JETSET and ARIADNE.

7 Properties of Events with Final State Photons

We now present our measurements in events with final state photons corrected for detector effects and the event selection. We consider four classes of distributions; the photon yield, the jet rates of the hadronic system, the properties of the photon itself, and those of the residual event. All properties examined depend on the y_{cut} applied. The yield and the jet rates are given for y_{cut} values between 0.005 and 0.2. For the other distributions we restrict ourselves to a low $y_{cut} = 0.005$ for which the uncertainty due to the energy and isolation cut is high, and a higher $y_{cut} = 0.06$ with a safer correction but limited sample size. We compare the yield to the predictions of the matrix element calculation [7] and QCD shower models [8, 9]. Photon and event properties are also compared to QCD shower models. In the latter case we normalise the predictions to the observed yield. This then provides a check that is largely independent of the yield. The uncertainties due to the energy and isolation requirement are not relevant for the comparisons of the data with shower models; JETSET was used to determine the correction factors and they were found to be almost identical with those from ARIADNE.

The contributions due to hadronic background and initial state photons are subtracted for all distributions.

7.1 The Cross Section

The cross section results have already been discussed in [2], where they were used to derive the electroweak coupling constants of up and down type quarks. For completeness we give a short summary of these results.

In table 1 and figs. 5a,b we show the fraction of all multihadronic events which contain final state photons as a function of y_{cut}. The yield decreases by about a factor of ten for an increase of y_{cut} from 0.005 to 0.2. It should be noted that the results for the different values of y_{cut} are correlated. The uncertainty in c_1 leads to a large systematic error of the cross section at very low y_{cut}. This uncertainty decreases rapidly with increasing y_{cut}. For $y_{cut} \geq 0.04$ the statistical error dominates. Also shown are the predictions from the matrix element calculation and the parton shower models JETSET and ARIADNE.

The ratio between data and the matrix element calculation and the parton shower models is displayed in figs. 5c,d and e. As stated before, we neglect the error on c_1 for the comparison of the data with the shower models. We make the following observations.

- The matrix element calculation is in good agreement with the data for $y_{cut} \leq 0.12$ but almost four standard deviations below the data at high y_{cut} (figure 5a,c).

y_{cut}	$(N_{\gamma+jets}/N_{had}) \cdot 10^3$	ME	JETSET	ARIADNE
0.005	5.95±0.44±0.77		4.67±0.07	6.15±0.03
0.010	4.78±0.36±0.53		3.76±0.06	4.88±0.02
0.020	3.66±0.28±0.29	$3.20^{+0.51}_{-0.11}$	2.85±0.06	3.67±0.01
0.040	2.32±0.21±0.10	$2.20^{+0.19}_{-0.04}$	1.99±0.04	2.58±0.01
0.060	1.72±0.17±0.08	$1.61^{+0.08}_{-0.02}$	1.53±0.03	1.98±0.01
0.080	1.28±0.14±0.06	$1.22^{+0.04}_{-0.01}$	1.19±0.03	1.57±0.01
0.100	1.04±0.13±0.05	$0.94^{+0.02}_{-0.01}$	0.97±0.02	1.29±0.01
0.120	0.89±0.12±0.04	$0.74^{+0.01}_{-0.00}$	0.82±0.01	1.11
0.140	0.80±0.11±0.04	0.59	0.70±0.01	1.00
0.160	0.70±0.10±0.03	0.47	0.62±0.01	0.90
0.180	0.64±0.10±0.03	0.37	0.57±0.01	0.83
0.200	0.67±0.10±0.03	0.30	0.54±0.01	0.80

Table 1: Photon selection for various y_{cut}. The corrected fraction of events with final state photons over the total number of hadronic events is listed. The first error combines the statistical and systematic uncertainty of c_2, added in quadrature, the second is due to the energy and isolation cut. Also shown are the predictions from the matrix element calculation [7] (ME) and the parton shower Monte Carlos JETSET [8] and ARIADNE [9]. The error on the matrix element prediction reflects the uncertainty of α_s. The uncertainties assigned to the JETSET and ARIADNE predictions are only due to variations of the QCD scale parameter Λ. Note that the second error of the data is not relevant for the comparison of the JETSET and ARIADNE prediction to the data.

This deviation is at least partly due to the different definitions of the retained events (see section 6.1). An approximate measure of this effect may be obtained if we correct the theoretical expectation according to the results of our analysis of the abelian matrix element. In this case a much better agreement between data and theory is found. Using the abelian model to correct the theoretical calculation, we find e.g. at y_{cut}=0.2, where the discrepancy is largest, that the expected photon yield increases from 0.30 to 0.48. A final assessment can only be made once our event definition can be adopted in a theoretical calculation.

- JETSET (figs. 5b,d) underestimates the photon yield at very low y_{cut} by 30% with a significance of about three standard deviations. For $y_{cut} \geq$0.06 the expectation is only 10% lower than the data and agrees within one standard deviation.

- ARIADNE (figs. 5b,e) reproduces the data at low y_{cut} but tends to overestimate the measured yield for $y_{cut} \geq$0.04 by about 25%. The significance of this discrepancy is up to two standard deviations.

7.2 Jet rates

7.2.1 Results and Comparison with Theoretical Expectations

The distribution of jets reflects the underlying parton structure and can therefore be directly compared with the QCD calculations. In the case of the inclusive hadronic event sample the fraction of n-jet events is very well described by matrix element calculations and by the QCD shower models of JETSET and ARIADNE.

In fig.6a we compare the relative jet rates with the parton shower models. JETSET tends to overestimate the observed two jet rate, or, equivalently, to underestimate the one jet rate for y_{cut} >0.06. ARIADNE describes the observed jet rates well. The data are currently not significant enough to discriminate between the models.

In table 2 and fig. 6b we display the absolute yield of one, two and three jet events with a hard photon. The number of events with three or more jets decreases rapidly with increasing y_{cut}, no such events are observed for $y_{cut} \geq$0.08. The fraction of two jet events increases slightly with y_{cut} for $y_{cut} \leq$0.02, and then decreases by almost an order of magnitude for an increase of y_{cut} up to 0.2. The yield of one jet events, i.e. events where the masses of all partons satisfy $M^2_{had}/E^2_{cm} < y_{cut}$ increases continuously with increasing y_{cut}. Also shown by the shaded bands are the expectations derived from the matrix element calculation; the widths indicate the uncertainty in α_s. While the two and three jet rates are in good agreement, the one jet yield at very high y_{cut} differs significantly from the theoretical prediction. For y_{cut}=0.20 the ratio of the expectation over the data is 0.25±0.08.

We have examined the one jet events for experimental biases by determining the recoiling hadronic mass taking advantage of the good measurement of the photon momentum and using the relation $y = 1 - x_\gamma$ with $x_\gamma = 2E_\gamma/E_{cm}$. True one jet events are to have $y < y_{cut}$. We find the assignment to be correct for typically 95% of the events. From the analysis with the abelian model of strong interactions we find that at least a large part of the discrepancy between data

y_{cut}	one jet	two jet	three jets	four jets
0.005	0.03± 0.02	1.78±0.24±0.25	2.65±0.27±0.34	1.27±0.18±0.15
0.010	0.03± 0.02	2.21±0.24±0.25	2.15±0.22±0.22	0.37±0.08±0.04
0.020	0.05±0.02	2.53±0.23±0.22	1.02±0.14±0.08	0.05±0.03
0.040	0.09± 0.03	2.03±0.19±0.11	0.20±0.06±0.01	
0.060	0.13± 0.04	1.54±0.15±0.05	0.06±0.03	
0.080	0.15± 0.04	1.13±0.13±0.03		
0.100	0.20±0.05±0.01	0.84±0.11±0.02		
0.120	0.24±0.06±0.01	0.65±0.10±0.02		
0.140	0.31±0.07±0.01	0.49±0.09±0.01		
0.160	0.34±0.07±0.01	0.36±0.07±0.01		
0.180	0.35±0.07±0.02	0.29±0.07±0.01		
0.200	0.42±0.08±0.02	0.25±0.06±0.01		

Table 2: The number of one, two and three jet events plus photons per 1000 multihadronic events are listed. The first error combines the statistical and systematic uncertainty of c_2, added in quadrature, the second is due to the energy and isolation cut.

y_{cut}	one jet	two jet	three jets	four jets
0.005	0.01±0.01	0.30±0.03±0.04	0.45±0.03±0.04	0.21±0.03±0.03
0.010	0.01±0.01	0.46±0.04±0.04	0.45±0.03±0.03	0.08±0.02±0.01
0.020	0.01±0.01	0.69±0.03±0.02	0.28±0.03±0.02	0.01 ±0.01
0.040	0.040±0.01	0.87±0.03±0.01	0.09±0.02± 0.01	
0.060	0.07±0.02	0.89±0.03±0.01	0.03±0.02	
0.080	0.12±0.03	0.88±0.03±0.01		
0.100	0.19±0.04	0.81±0.04±0.01		
0.120	0.27±0.06±0.01	0.73±0.06±0.01		
0.140	0.38±0.06±0.01	0.62±0.06±0.01		
0.160	0.49±0.07±0.01	0.51±0.07±0.01		
0.180	0.55±0.07±0.01	0.45±0.07±0.01		
0.200	0.62±0.07±0.01	0.38±0.07±0.01		

Table 3: The fractions of one, two and three jet events plus photon are listed. The first error combines the statistical and systematic uncertainty of c_2, added in quadrature, the second is due to the energy and isolation cut.

and calculation can be explained by the different event definitions. Again, a final assessment can only be made once our event definition can be adopted in a theoretical calculation.

We can use the relatively strong dependence on α_s of the two and three jet rates at low y_{cut} to determine the value of the strong coupling constant. To reduce systematic uncertainties and to be independent of unknowns in the overall production rate we use the ratio of three jet events over the sum of two and three jet events. For two different values of $y_{cut} = 0.02$; 0.04 we find

$$\frac{\sigma_{\gamma+3j}}{\sigma_{\gamma+2j} + \sigma_{\gamma+3j}} = 0.287 \pm 0.020; \quad 0.090 \pm 0.018.$$

Translating these ratios into values of a first order $\alpha_s^{(1)}$ leads to

$$\alpha_s^{(1)} = 0.161 \pm 0.012; \quad 0.154^{+0.031}_{-0.025}$$

for the two y_{cut} values respectively. These results are in good agreement with the $\alpha_s^{(1)}$ value of 0.177±0.013 obtained from the inclusive multihadronic event sample. In the absence of differential distributions for photon plus n-jet events we cannot calculate the uncertainties from the hadronisation and recombination mechanism which are important for the uncertainty of the $\alpha_s^{(1)}$ value from the multihadronic jet rates.

7.2.2 Comparison with Jet Rates in the Inclusive Multihadronic Event Sample

It has been suggested [7, 23] that a comparison of the cross sections for the production of $q\bar{q}g$ events from the total multihadronic sample to events with two jets and a photon ($q\bar{q}\gamma$) can provide information on the strength and structure of the strong interactions. The idea is to use the well known properties of photon radiation to disentangle the specific QCD contributions.

The corresponding cross sections for $q\bar{q}g$ and $q\bar{q}\gamma$ events are given by [24]

$$\sigma(q\bar{q}g)(y_{cut}) \propto C_F \frac{\alpha_s}{2\pi} B(y_{cut}) + (\frac{\alpha_s}{2\pi})^2 C_F [C_F h_c(y_{cut}) + N_c h_N(y_{cut}) + \frac{N_f}{2} h_T(y_{cut})] \quad (5)$$

$$\sigma(q\bar{q}\gamma)(y_{cut}) \propto A_c [\frac{\alpha}{2\pi} B(y_{cut}) + \frac{\alpha}{2\pi}\frac{\alpha_s}{2\pi} C_F h_c(y_{cut})] \quad (6)$$

where α_s and α are the strong and electromagnetic coupling strengths, $C_F = 4/3$ is the colour factor, $N_c = 3$ the number of colours and N_f the number of flavours. Assuming the contributions of up and down type quarks to agree with the standard model with an electroweak mixing angle $\sin^2\theta_w$=0.23, the average squared quark charge A_c has the value 0.2249. The functions $f(y_{cut})$ reflect the topological configurations of the parton/photon states. They account for single bremsstrahlung (B), double bremsstrahlung (h_c), the non-abelian contribution (h_N), and the gluon splitting into a quark pair (h_T). Since photons couple to quarks in the same way as gluons (apart from the strength), $B(y_{cut})$ and $h_c(y_{cut})$ are almost identical for gluon and photon emission. The terms for the gluon self coupling and for the gluon splitting are unique to the three jet distribution. The combination of (5) and (6) proposed in [7] is a convenient way to separate the common contributions from those specific to the QCD process.

$$R_{\gamma g} = \frac{\alpha A_c}{C_F} \frac{\sigma(q\bar{q}g)}{\sigma(q\bar{q}\gamma)} = \alpha_s [1 + \frac{\alpha_s}{2\pi} \frac{N_c h_N(y_{cut}) + \frac{N_f}{2} h_T(y_{cut})}{B(y_{cut}) + (\alpha_s/2\pi) C_F h_c(y_{cut})}] \quad (7)$$

The h_c term is expected to contribute about 10% to $R_{\gamma g}$ at y_{cut}=0.06. Those for the self coupling (h_N) and for $q\bar{q}q\bar{q}$ (h_T) are significant with $N_c h_N \sim 4 \cdot \frac{N_f}{2} h_T$. Given that the single bremsstrahlung $B(y_{cut})$ term is well known, this implies (7) is particularly sensitive to the structure of the triple gluon vertex (h_N).

We will now use this ratio to measure α_s. This measurement is strongly correlated with the determination of α_s from three jet event rate alone. In using jet rates the three jet cross section (5) is related to the overall event yield which is well known and depends only weakly on α_s. In using $R_{\gamma g}$ we relate (5) to the precisely known values of α and $\sin^2\theta_w$ (assuming standard model couplings). The precision of the ratio $R_{\gamma g}$ is currently limited by the statistical and systematic accuracy of the photon events. The errors on α_s derived from the three jet fraction are given, essentially, by the uncertainties in the recombination scheme, the hadronisation correction and the scale dependence [18]. In the absence of a differential parton distribution for $q\bar{q}\gamma$ events these uncertainties cannot be estimated.

Neglecting α_s^2-terms we can use our measurement of $R_{\gamma g}$ to determine α_s in first order. For y_{cut}=0.06, where we have the largest sensitivity, we find

$$\alpha_s^{(1)} \;=\; 0.195 \pm 0.020$$

again in agreement with the previously mentioned value determined from the three jet fraction in the inclusive hadronic event sample. The result also agrees with our measurement of $\alpha_s^{(1)}$ from the relative rates of two and three jet plus photon events, discussed in section 7.2.1. In using (7) to determine α_s in second order we have to be aware that the α_s value in the h_c term stems from (6) and is of *first* order but all other values of α_s are of *second* order and come from the cross section for three jet events (5). In obtaining $\alpha_s^{(2)}$ from (7) we set $\alpha_s^{(1)} = \alpha_s^{(2)}$. Since $\alpha_s^{(1)}$ enters only in the h_c term this leads to a small ($\sim$ 5%) correction. In fig. 7a we display the observed ratio $R_{\gamma g}$ as a function of $\alpha_s(M_{Z^0})$ according to equation 7 and translate our measurement into

$$\alpha_s^{(2)}(M_{Z^0}) \;=\; 0.122 \pm 0.010$$

in agreement with the α_s of 0.118 ± 0.08 obtained from the topology of hadronic events alone. The dominant contribution to the error is from theoretical ambiguities, the pure experimental uncertainty is 0.003 [18].

Another test of the QCD structure is given by the y-dependence of $R_{\gamma g}$. For low y_{cut} the positive contributions from the gluon self coupling tend to compensate the negative contribution of the double bremsstrahlung term, leading to a *increase* of the ratio at low y_{cut} [7]. For N_c=0, i.e. the absence of the self coupling, the ratio would exhibit a slow *decrease*. At large y_{cut}, theory predicts an almost flat behaviour, over a wide range of α_s values, i.e.

$$\frac{N_c h_c(y_{cut}) \;+\; \frac{N_f}{2} h_T(y_{cut})}{B(y_{cut})} \;\sim\; constant.$$

This dependence is shown in fig. 7b for the data together with the expectation for various values of α_s. The data show almost no variation with y_{cut} for $y_{cut} \geq 0.04$ in agreement with QCD. However, for $y_{cut} < 0.06$ $R_{\gamma g}$ increases with decreasing y_{cut} in agreement with a non-abelian theory of strong interactions. The abelian expectation (displayed for α_A=0.2) does not describe the data.

7.3 Properties of the Photon

We now turn to the properties of the photon itself. As yet no matrix element calculation exists for these properties and we can compare our measurement only with the parton shower models JETSET and ARIADNE. These models assume a time sequence in the parton branchings with a decreasing virtuality of the quark system in each step of the shower process. The transverse momentum of the photon with respect to the emitting quark is therefore a measure of the time scale of the emission (see also discussion in [23]): energetic photons produced at large angles stem from quarks or parton systems of high virtual masses and are, therefore, emitted at an early stage of the jet development. Within the JETSET program typically 90% of the photons retained by our cuts for y_{cut}=0.04-0.16 are emitted in the *first* branching, i.e. before any gluon radiation. This number decreases to 75% at y_{cut}=0.005 and to 81% at y_{cut}=0.2. The photon properties are therefore related to the jet evolution and provide information about the masses involved in the parton branching. Because of the conceptual simplicity and the general success of this model of jet evolution we will frequently refer to it.

In the following, we restrict ourselves to y_{cut} values of 0.005 and 0.06 and present distributions corrected for detector effects and our selection criteria. We have verified that these corrections are consistent for JETSET and ARIADNE. This implies in particular that the uncertainties due to the energy and isolation requirements are unimportant for the comparison of data and these models. The corrections can be large in certain kinematical regions and, as discussed in section 5, can imply substantial systematic uncertainties in the shape of the distribution. This is particularly true for y_{cut}=0.005, whereas the corrections are in general slowly varying for y_{cut}=0.06. Systematic uncertainties due to the energy and isolation requirement and due to detector effects are indicated by the dashed error bars in figs. 8-15. These plots are normalised to their numbers of entries. We list the observed average values of the distributions together with the expectations from the two QCD shower models in table 4.

7.3.1 The Photon Energy

Figure 8 shows the photon energy spectrum for the two values of y_{cut}. For y_{cut}=0.005 the photon yield decreases by about a factor 10 for an increase of the energy from 7.5 to about 45 GeV. The energy distribution is much flatter for y_{cut}=0.06 due to the larger photon-jet mass required.

The predictions of JETSET and ARIADNE are consistent with each other and are in agreement with the data.

7.3.2 The Transverse Momentum with Respect to the Thrust Axis

The transverse momentum distribution of the photon with respect to the thrust axis p_T^{thr} is displayed in fig. 9. The thrust has been calculated from all charged tracks and clusters in the electromagnetic calorimeter, including the photon candidate. From leading order calculations we expect the distribution to be proportional to $1/p_T^{thr}$. Kinematically, the transverse momentum is limited to $1/\sqrt{3}E_{beam}$ ~27 GeV. Since the thrust axis is a good measure of the direction

Property	y_{cut}	Data	JETSET	ARIADNE
Photon Energy (GeV)	0.005	19.7±0.6	20.3±0.1	20.7±0.1
	0.060	23.2±0.8±0.1	23.2±0.1	24.1±0.1
p_T wrt Thrust (GeV)	0.005	6.18±0.27	6.48±0.03	6.45±0.03
	0.060	10.6±0.4	11.0±0.1	10.5±0.1
p_T wrt Jet (GeV)	0.005	10.6±0.5±0.2	11.1±0.1	11.3±0.1
	0.060	18.8±0.8±0.1	19.4±0.1	18.8±0.1
Angle wrt Jet (deg)	0.005	68.3±2.1±0.3	73.3±0.8	71.7±0.2
	0.060	84.1±2.6±0.3	92.5±0.3	94.9±0.3
Jet/Photon Mass (GeV)	0.005	15.2±0.5±0.1	15.1±0.1	14.9±0.1
	0.060	33.3±0.9±0.4	36.7±0.2	38.2±0.2
Mass Photon Hemisphere(γ incl)(GeV)	0.005	22.2±0.5±0.1	21.7±0.1	21.2±0.1
	0.060	27.5±0.9±0.1	27.6±0.1	26.6±0.1
Mass Photon Hemisphere(γ excl)(GeV)	0.005	11.9±0.4±0.1	10.8±0.1	10.4±0.1
	0.060	9.5±0.5±0.1	8.9±0.1	8.5±0.1
Mass non-Photon Hemisphere (GeV)	0.005	16.1±0.5±0.1	15.5±0.1	15.4±0.1
	0.060	16.1±0.7±0.1	16.6±0.1	16.4±0.1

Table 4: Average values of photon and event properties in the data and for JETSET and ARIADNE. The first error for the data is the statistical and experimental systematic, the second is due to the energy and isolation cut. The errors in the model predictions are statistical only.

of the primary quarks, the p_T is related to the mass of the primary quark with $p_T \sim M_q/2$ assuming the photon stems from the first emission.

Also shown in figs. 9a,b are the expectations from ARIADNE and JETSET. The data and the predictions have a maximum at $p_T \sim \sqrt{y_{cut}} \cdot E_{cm}/2 \sim M_q^{min}/2$, i.e. 3 and 11 GeV for the two values of y_{cut}. For larger p_T the fall off is consistent with the leading order expectation. For y_{cut}=0.06 there is an enhancement at low p_T due to highly energetic photons that determine the thrust direction. ARIADNE and JETSET predict different fractions of these low p_T events at y_{cut}=0.06. In JETSET there are 12.9±0.4% of events with $p_T < 2.5$ GeV, in ARIADNE 15.9±0.4%. We observe 14.3±3.6±1.8%, consistent with both predictions.

7.3.3 Transverse Momentum with Respect to the Jet Direction

A more direct relation between the mass of the emitting quark and of the photon is expected for the transverse momentum with respect to the direction of the jet with minimal jet-photon mass, p_T^{jet}. The corresponding distribution is shown in fig. 10.

For the two y_{cut} values the measured p_T^{jet} distributions peak at values of 2.5 and 12.5 GeV, similar to those for the p_T^{thr}. For p_T^{jet} the kinematic limit is close to E_{beam} which corresponds to a topology where the associated jet is soft and is emitted almost perpendicular to the thrust direction. For low values of p_T^{jet} and y_{cut}=0.06 the two models predict different yields. JETSET predicts 4.8±0.3%, whereas ARIADNE predicts 7.6±0.4% of these events to have p_T^{jet} smaller than 5 GeV. We observe the low p_T^{jet} photons in 7.0±2.5±2.3% of events. This small p_T^{jet} for

a y_{cut} of 0.06 implies that the residual hadronic system is in the opposite hemisphere to the photon. These events are the one jet events discussed already in section 7.2.

7.3.4 Angle with Respect to the Jet

The angle between the photon and the jet with the minimal jet-photon mass α^{jet} shown in fig. 11 is strongly correlated to p_T^{jet}. It is strongly biased by our isolation requirement on the photon candidate. We accept essentially no events with $\alpha^{jet} \leq 20$ degrees for y_{cut}=0.005, or 50 degrees for y_{cut}=0.06.

For y_{cut}=0.005, we observe an almost linear decrease of the yield with increasing angle, whereas the distribution peaks at $\alpha^{jet} \sim 80$ degrees for y_{cut}=0.06. The bulk of the data are well described by both JETSET and ARIADNE. However, there is a significant difference between the two models for $170 < \alpha^{jet} < 180$ degrees for y_{cut}=0.06. This region is almost identical to the topology of $p_T \sim 0$ GeV with respect to the jet axis discussed in the previous section.

7.3.5 Jet Photon Mass

Fig. 12 shows the minimum mass of the photon and a jet. It was calculated using the relation to obtain the value for y: $M_{\gamma,jet} = \sqrt{2E_{jet}E_{\gamma}(1-\cos\alpha^{jet})}$ with α^{jet} the angle between photon and jet.

JETSET and ARIADNE describe the data well, however they predict different yields for masses $M_{\gamma,jet} \sim E_{cm}$ at y_{cut}=0.06. Again these events are one jet events and the difference has been discussed in section 7.3.3.

7.4 Hemisphere Masses

We next turn to a direct investigation of the hadronic systems of these events. We compare the hemisphere masses with respect to the thrust direction in the data and the models. This analysis is also motivated by the jet development as seen in the shower models. For emissions at an early stage of the cascade, a quark q_1 decays either into a quark q_1' and a photon with a recoiling quark q_2, or (in ARIADNE) an electric dipole between q_1 and q_2 emits a photon changing the quark configuration into q_1' and q_2'. The kinematics in these models involve the masses of q_1, q_1' and q_2' on which the hemisphere masses depend. The structure of the branchings is determined by Sudakov form factors and the α_s value at the appropriate scale. In this section we determine the hemisphere masses from all final state *particles*, i.e. we do not correct back to the parton level.

7.4.1 Total Mass in Photon Hemisphere

We first consider the total mass of the hemisphere containing the photon

$$M_{in,\gamma} = \sqrt{(E_\gamma + \Sigma E_{had})^2 - (\vec{p}_\gamma + \Sigma \vec{p}_{had})^2}$$

where the index *had* refers to all particles in a hemisphere apart from the photon. In the picture given above, this corresponds to the properties of q_1. In fig. 13 $M_{in,\gamma}$ is displayed.

The distributions show a maximum at $M_{in,\gamma} \sim 20$ GeV and 30 GeV for the two values of y_{cut}. The larger mass for the higher y_{cut} values reflects the bias from the higher required mass in the y_{cut} selection. For y_{cut}=0.005 the average mass is significantly larger than the minimum allowed photon-*jet* mass of $\sqrt{y_{cut}} \times E_{cm}$, indicating the presence of additional jets in this hemisphere (cf. section 7.2). For y_{cut}=0.06 the maximum is only slightly larger. The contributions at $M_{in,\gamma} \leq 20$ GeV are due to particles which are scattered into the photon hemisphere although the associated jet is directed into the opposite one. The predictions of JETSET and ARIADNE agree well with the measurements for both y_{cut} values.

7.4.2 Mass in the Photon Hemisphere Excluding the Photon

In fig. 14 we show the corresponding mass $M_{ex,\gamma}$ calculated as for 7.4.1 but excluding the photon. This should be related to the mass of the quark q_1'. The observed distribution is rather independent of the y_{cut} applied apart from a tail to larger masses for y_{cut}=0.005 due to the larger available phase space. This agreement for the two values of y_{cut} suggests that the QCD evolution is not significantly changed by the photon emission as expected by the colour blindness of the photon. The two shower models are consistent with the data although ARIADNE tends to have smaller masses.

7.4.3 Mass in the Hemisphere not Containing the Photon

The mass in the thrust hemisphere not containing the photon is also similar for the two values of y_{cut} (figs. 15a,b). They are larger than the hadronic masses in the photon hemisphere due to the larger phase space available. On the other hand, they are smaller than $M_{in,\gamma}$ since the latter is biased due to the requirement on the photon.

Both QCD shower models reproduce the data well.

8 Summary

In this paper we have discussed several tests of QCD using final state photons as a tool to isolate the gluon contributions.

From the production rate of events with two jets plus photon with that for three jet events we determine α_s in second order as

$$\alpha_s^{(2)} = 0.122 \pm 0.010.$$

The error contains only statistical and experimental systematic errors, but no contributions from uncertainties in the recombination scheme, the fragmentation and the scale dependence. The value agrees with the $\alpha_s^{(2)}$ obtained from the inclusive hadronic event sample, but the measurements are correlated. The y-dependence of the ratio is sensitive to the structure of the triple gluon vertex. Our data agree with the QCD expectation and cannot be described by a model with an abelian strong interaction.

Although the QCD shower models JETSET and ARIADNE are in agreement with each other and with the data over a wide range of centre-of-mass energies for the inclusive multihadronic event sample, there are significant differences in the yield and in the jet rates in events with a final state photon. These differences might be caused by the different treatment of the parton evolution in the two programs. For the yield ARIADNE gives a good account of the data at low y_{cut} values but tends to overestimate it at high y_{cut} values ($\leq$ 2 standard deviations). The jet rates are well described by ARIADNE. JETSET predicts a yield which is about three standard deviations lower than the data at low y_{cut} and tends to overestimate the jet multiplicities (about 1.5 standard deviations). We have also examined the properties of the photons. Their energies and relations to jets as well as the masses of the event hemispheres including and opposite to the photon are well reproduced by both Monte Carlo models.

Acknowledgements

We are grateful to G.Kramer, B.Lampe, L.Lönnblad, T.Sjöstrand and P.Zerwas for many inspiring discussions.

It is a pleasure to thank the SL Division for the efficient operation of the LEP accelerator, the precise information on the absolute energy, and their continuing close cooperation with our experimental group. In addition to the support staff at our own institutions we are pleased to acknowledge the
Department of Energy, USA,
National Science Foundation, USA,
Science and Engineering Research Council, UK,
Natural Sciences and Engineering Research Council,Canada,
Israeli Ministry of Science,
Minerva Gesellschaft,
Japanese Ministry of Education, Science and Culture (the Monbusho) and a grant under the Monbusho International Science Research Program,
American Israeli Bi-national Science Foundation,
Direction des Sciences de la Matière du Commissariat à l'Energie Atomique, France,
Bundesministerium für Forschung und Technologie, FRG,
A.P. Sloan Foundation and Junta Nacional de Investigação Científica e Tecnológica, Portugal.

References

[1] OPAL-Collaboration, M. Z. Akrawy et al., Phys. Lett. B246 (1990) 285.

[2] OPAL-Collaboration, G. Alexander et al., Phys.Lett. B264 (1991) 219.

[3] ALEPH-Collaboration, D. Decamp et al., CERN-PPE 91-89.

[4] DELPHI-Collaboration, P. Abreu et al., CERN-PPE 91-174.

[5] F. Boudjema et al., in Proceedings of the Workshop on Z-Physics at LEP 1, ed. G. Altarelli, R. Kleiss, and C. Verzegnassi, CERN 89-08.

[6] P. Mättig and W. Zeuner, Z. Phys. C52 (1991) 37.

[7] G. Kramer and B. Lampe, DESY 91-078.

[8] T. Sjöstrand, Comp. Phys. Comm. 39 (1986), 347; JETSET, Version 7.2.

[9] U. Petterson, LU TP 88-5 (1988), U. Petterson, L. Lönnblad, LU TP 88-15 (1988), L. Lönnblad LU TP 89-10 (1988), L. Lönnblad, ARIADNE3.2 and private communication; contribution to the MC-Workshop Amsterdam, April 1991

[10] OPAL-Collaboration, K. Ahmet et al. Nucl. Inst. Meth. A305 (1991) 275.

[11] JADE-Collaboration, W. Bartel et al., Z. Phys. C33 (1986) 23; JADE-Collaboration, S. Bethke et al., Phys. Lett. B123 (1988) 235.

[12] OPAL-Collaboration, M. Z. Akrawy et al., Phys. Lett. B253 (1991), 511.

[13] F. A. Berends, R. Kleiss, S. Jadach, Nucl. Phys. B202 (1982), 63.

[14] R. Brun et al., GEANT3 User's Guide, CERN DD/EE/84-1 (1989); D. R. Ward, Proc. MC'91 Workshop, NIKHEF, Amsterdam 1991. J. Allison et al., Comp. Phys. Comm. 47 (1987) 55

[15] OPAL-Collaboration, M. Z. Akrawy et al., Phys. Lett. 241B (1990) 133.

[16] OPAL-Collaboration, G. Alexander et al., Phys. Lett. 261B (1991) 334.

[17] Private communication Y. Dokshitzer, R. Kleiss, and P. M. Zerwas.

[18] OPAL-Collaboration, M. Z. Akrawy et al., Z. Phys. C49 (1991) 375.

[19] G. Kramer and N. Magnusson, Z. Phys. C49 (1991) 301.

[20] G. Altarelli and G. Parisi, Nucl. Phys. B216 (1977) 298.

[21] T. Sjöstrand, Int. J. of mod. Phys. A3 (1988) 751.

[22] OPAL-Collaboration, M. Z. Akrawy et al., Z. Phys. C47 (1990) 505.

[23] E. Laermann, T. F. Walsh, I. Schmitt and P. M. Zerwas, Nucl. Phys. B207 (1982), 205.

[24] G. Kramer and B. Lampe, Fortschr. Phys. 37 (1989) 161.

Figure Captions

Figure 1: Feynman diagram for final state photon emission.

Figure 2: (a) Event efficiency as a function of y_{cut}; (b) efficiency ϵ_1 as a function of the photon energy for y_{cut}=0.005 (c) efficiency ϵ_1 as a function of the photon energy for y_{cut}=0.06, circles: JETSET, squares: ARIADNE;

Figure 3: (a) Uncorrected spectrum of the photon energy for y_{cut}=0.005. Indicated are the data (points with error bars), the normalised prediction by JETSET (light grey) and the background contribution (dark grey); (b) Distribution of the polar angle $\cos\theta$ of the photon candidate for y_{cut}=0.005. Indicated are the data (points with error bars) and the normalized prediction by JETSET (light grey).

Figure 4: Distribution of the smallest angle of a particle with respect to the photon for y_{cut} =0.005 (a) and y_{cut}=0.06 (b); (c) Acolinearity angle of the two jets from two jets plus photon events, after boosting them into the hadronic rest frame. For details see text; (d) energy resolution of the jet reconstruction as defined in the text. The points with error bars represent the data, the grey area is the prediction of JETSET after a detector simulation.

Figure 5: (a) Number of events with final state photons per 1000 multihadronic events (points with error bars) compared to the matrix element calculation, the grey band represents the uncertainty due to α_s; (b) Number of events with final state photons per 1000 multihadronic events (points with error bars) compared to JETSET (full line) and ARIADNE (dotted line); here the error of the data points does not contain contributions from the requirements on the energy and and isolation cone. Ratio of prediction/data (c) for matrix element calculation, (d) JETSET and (e) ARIADNE. Note that the results for the various y_{cut} values are correlated.

Figure 6: (a) Relative jet rates compared to JETSET (full line) and ARIADNE (dotted line); (b) Absolute one, two and three jet rates compared to the matrix element calculation, the grey bands represent the uncertainties due to α_s

Figure 7: (a) Expectation of the ratio $R_{\gamma g}$ as a function of α_s for y_{cut}=0.06 (full line). The horizontal band represents the one standard deviation range of the measured value of $R_{\gamma g}$. Its intersection with the curve determines the range of α_s (vertical band); (b) $R_{\gamma g}$ as a function of y_{cut}, points with error bars: data, full lines: predictions for different values of α_s, dotted line: prediction from an abelian model of QCD.

Figure 8: Corrected photon spectrum (a) y_{cut}=0.005, (b) y_{cut}=0.06. Points with error bars: data, full line: JETSET, dotted line: ARIADNE. The dashed error bars include the additional systematic error due to the energy and isolation cuts.

Figure 9: Transverse momentum p_T^{thr} of the photon with respect to the thrust axis for (a) y_{cut}=0.005 and (b) y_{cut}=0.06. Points with error bars: data, full line: JETSET, dotted line: ARIADNE. The dashed error bars include the additional systematic error due to the energy and isolation cuts.

Figure 10: Transverse momentum p_T^{jet} of the photon with respect to the jet with the minimal photon-jet mass for (a) y_{cut}=0.005 and (b) y_{cut}=0.06. Points with error bars: data, full line: JETSET, dotted line: ARIADNE. The dashed error bars include the additional systematic error due to the energy and isolation cuts.

Figure 11: Angle of the photon with respect to the jet with the minimal photon-jet mass for (a) y_{cut}=0.005 and (b) y_{cut}=0.06. Points with error bars: data, full line: JETSET, dotted line: ARIADNE. The dashed error bars include the additional systematic error due to the energy and isolation cuts.

Figure 12: Minimal photon-jet mass in GeV (a) y_{cut}=0.005, (b) y_{cut}=0.06. Points with error bars: data, full line: JETSET, dotted line: ARIADNE. The dashed error bars include the additional systematic error due to the energy and isolation cuts.

Figure 13: Invariant mass of all particles including the photon in the photon hemisphere for (a) y_{cut}=0.005 and (b) y_{cut}=0.06. Points with error bars: data, full line: JETSET, dotted line: ARIADNE. The dashed error bars include the additional systematic error due to the energy and isolation cuts.

Figure 14: Invariant mass of all particles except in the photon hemisphere for (a) y_{cut}=0.005 and (b) y_{cut}=0.06. Points with error bars: data, full line: JETSET, dotted line: ARIADNE. The dashed error bars include the additional systematic error due to the energy and isolation cuts.

Figure 15: Invariant mass of all particles in the hemisphere not containing the photon for (a) y_{cut}=0.005 and (b) y_{cut}=0.06. Points with error bars: data, full line: JETSET, dotted line: ARIADNE. The dashed error bars include the additional systematic error due to the energy and isolation cuts.

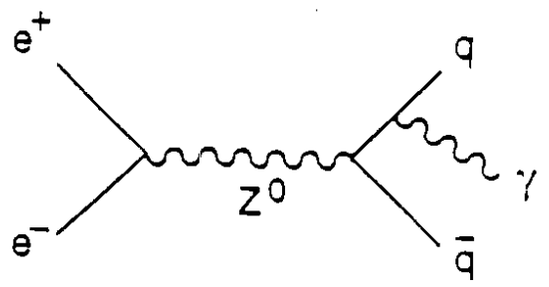

Figure 1

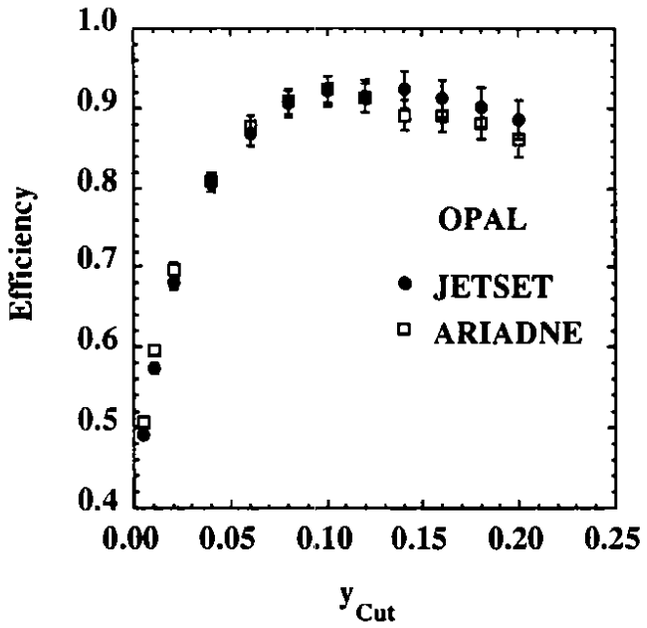

Figure 2a

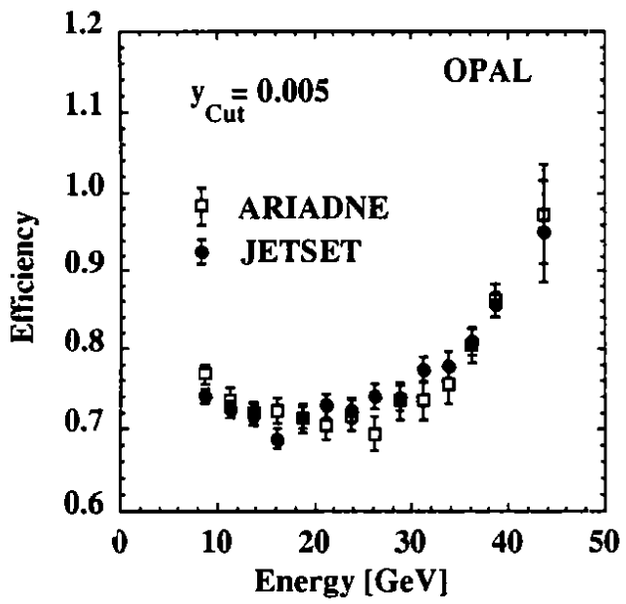

Figure 2b

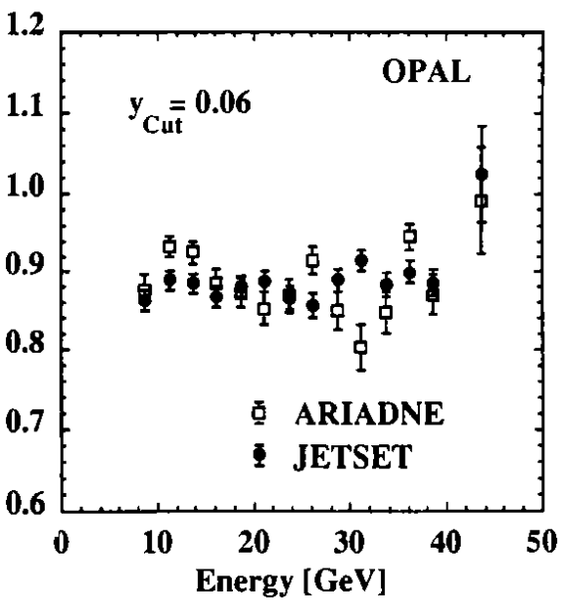

Figure 2c

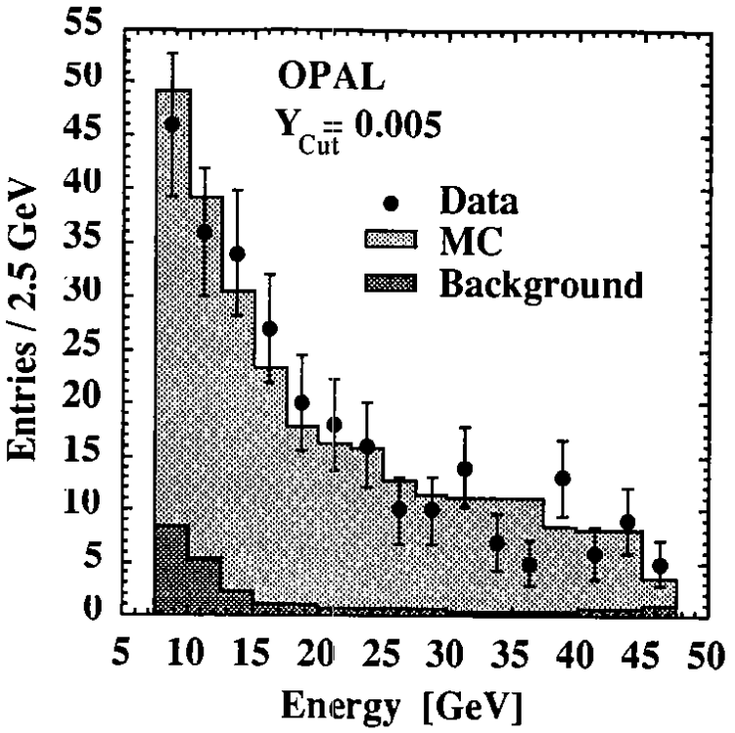

Figure 3a

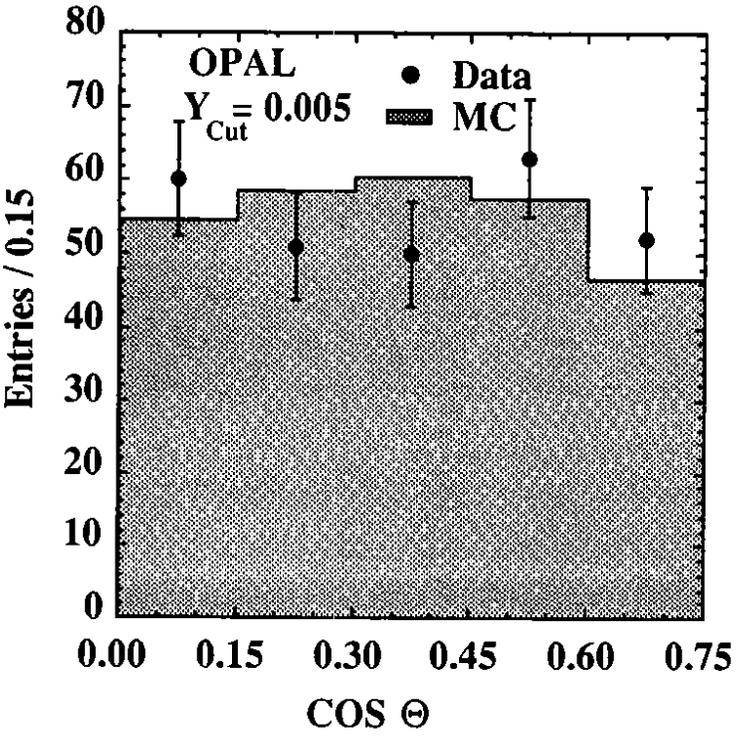

Figure 3b

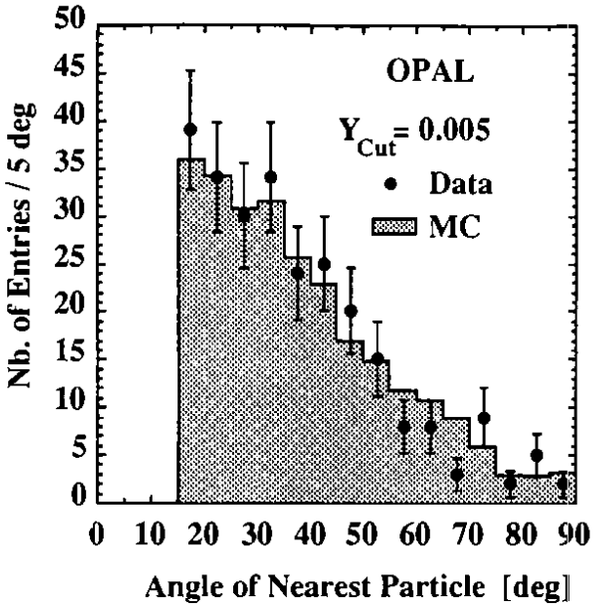

Figure 4a

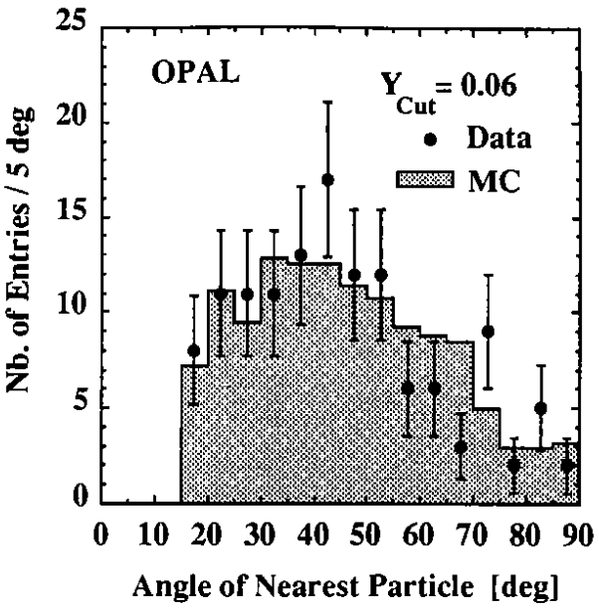

Figure 4b

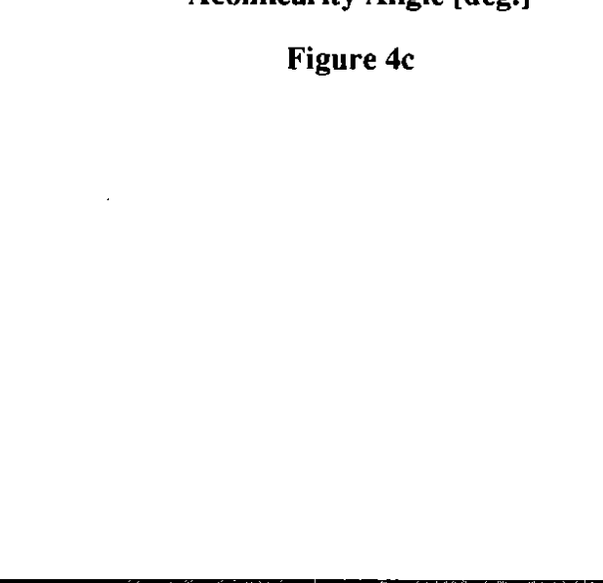

Figure 4c

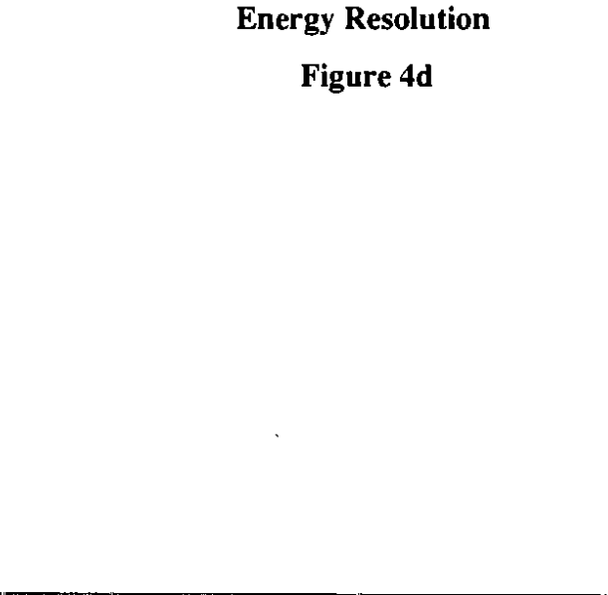

Figure 4d

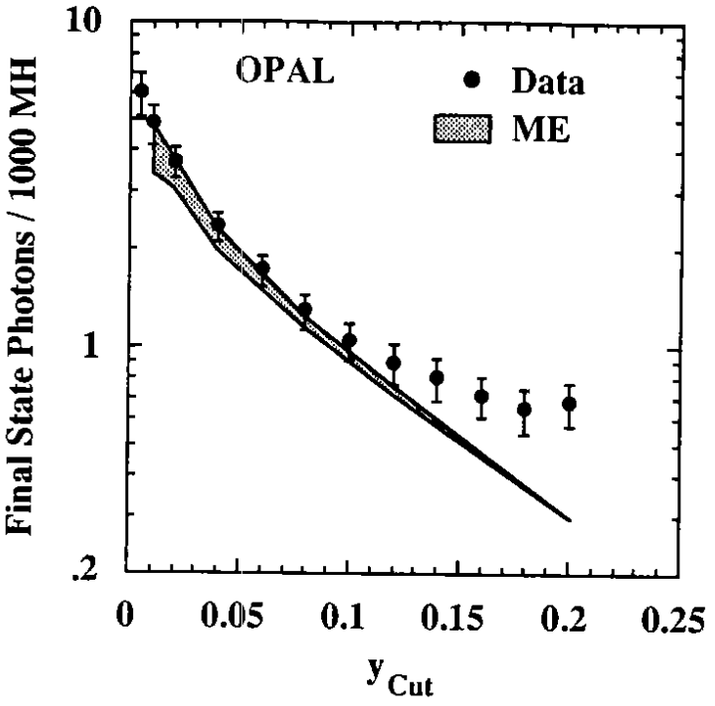

Figure 5a

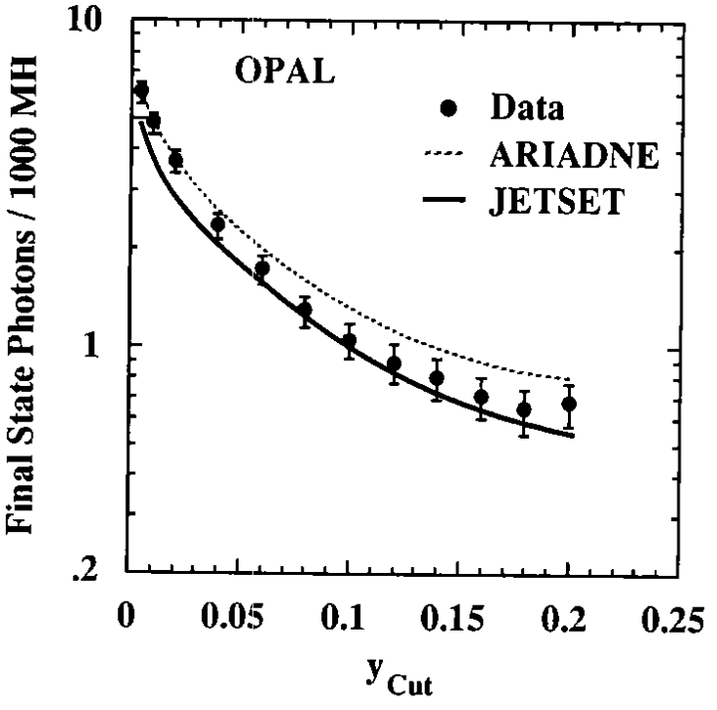

Figure 5b

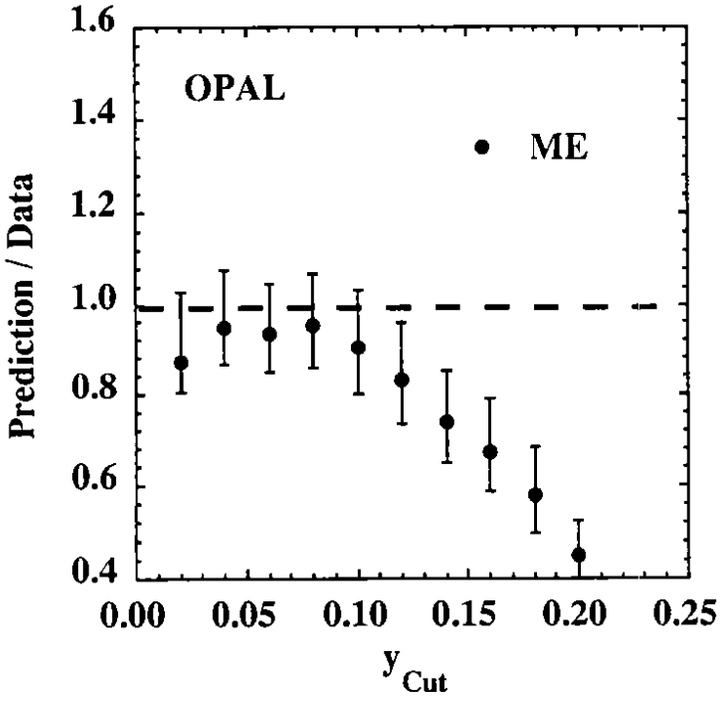

Figure 5c

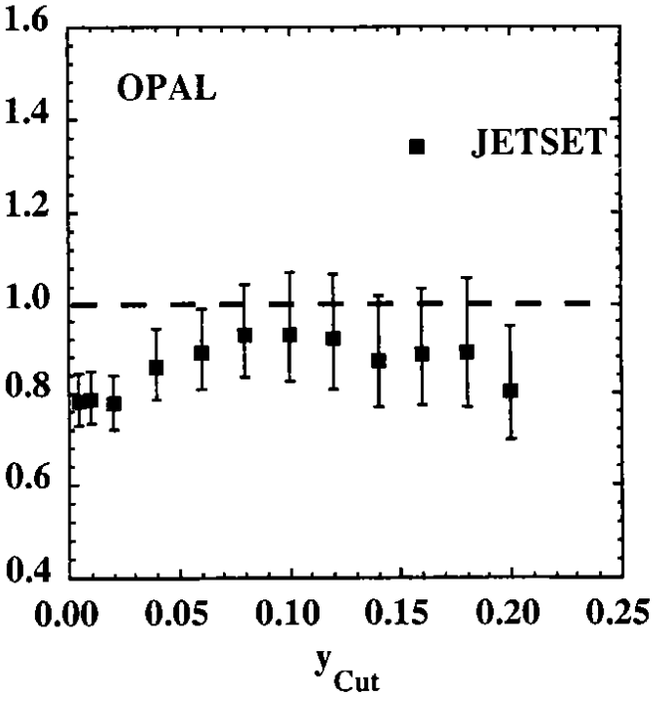

Figure 5d

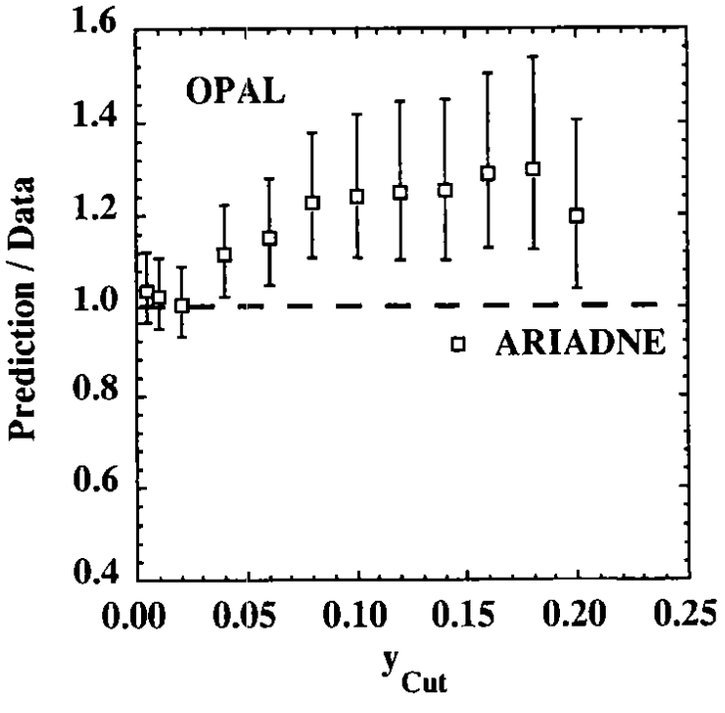

Figure 5e

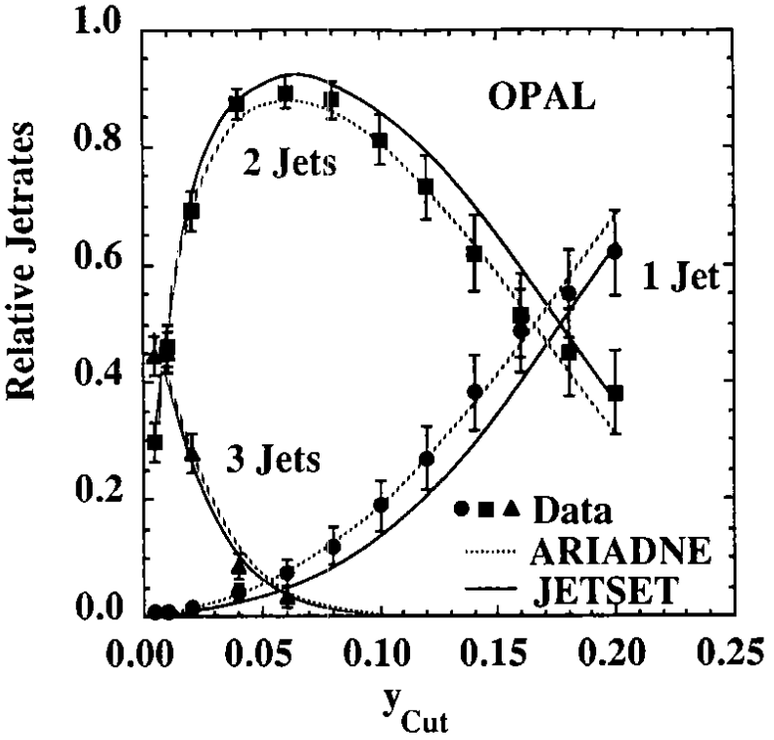

Figure 6a

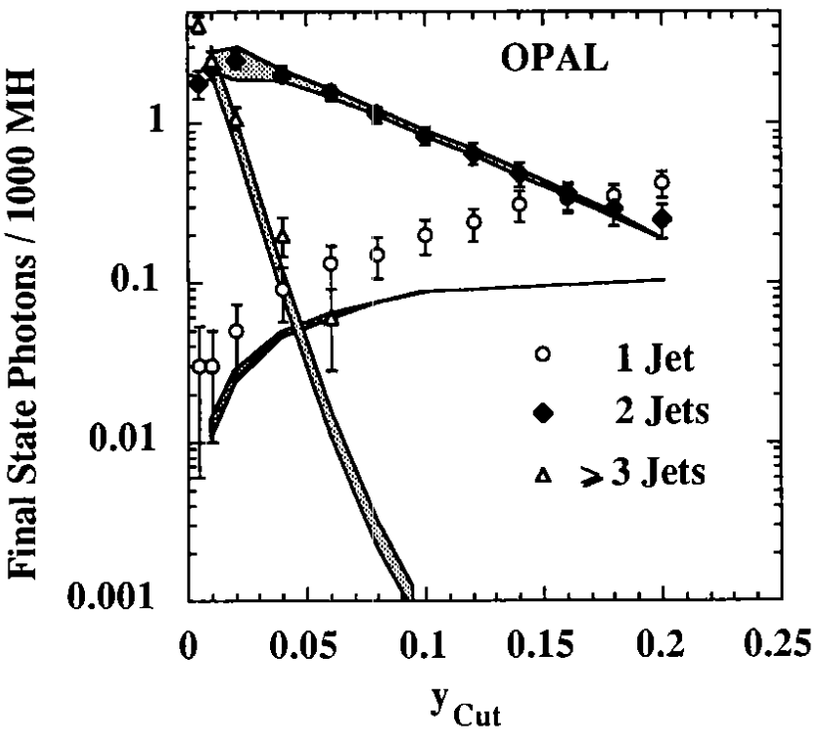

Figure 6b

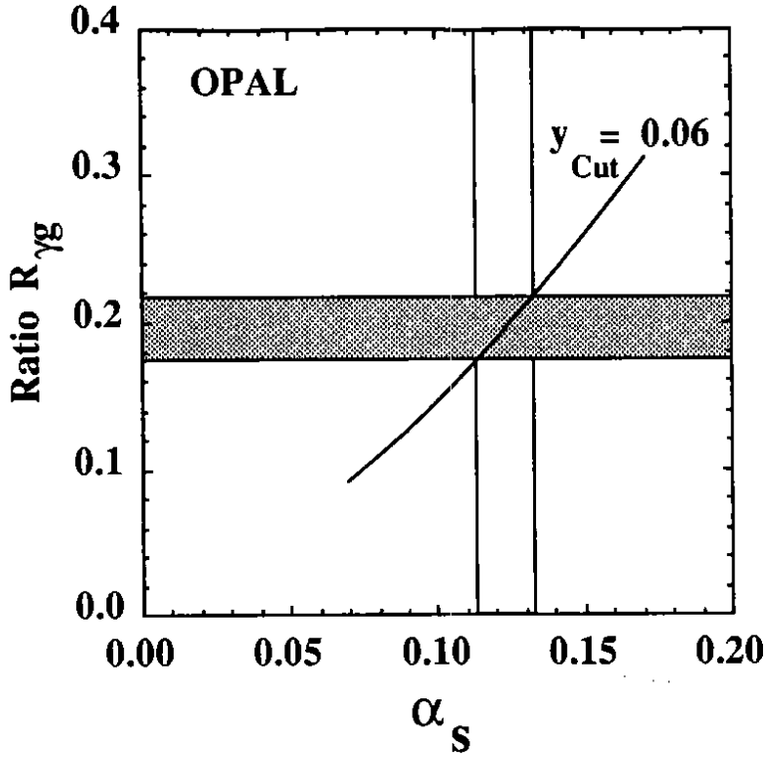

Figure 7a

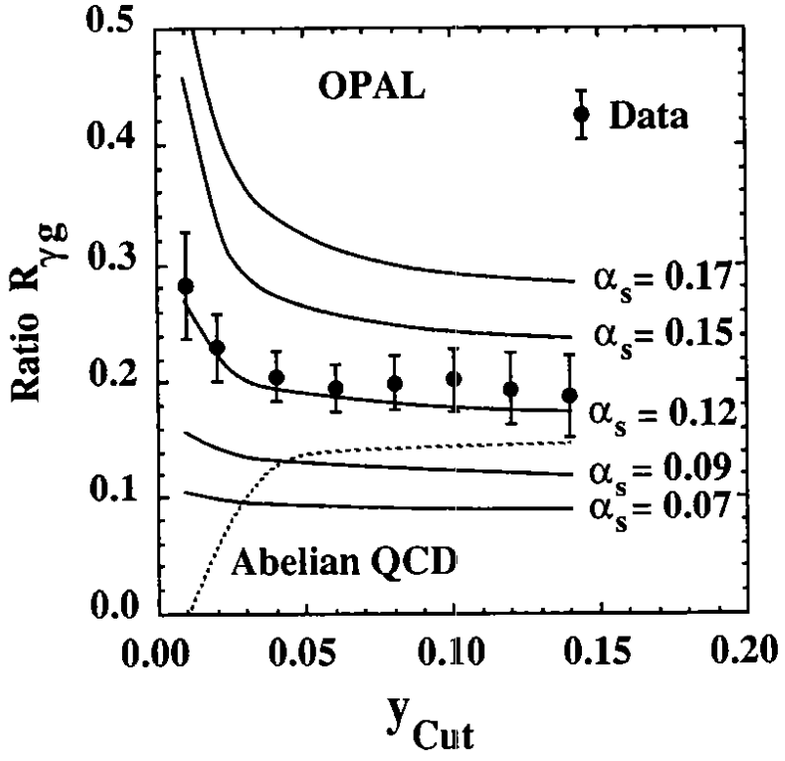

Figure 7b

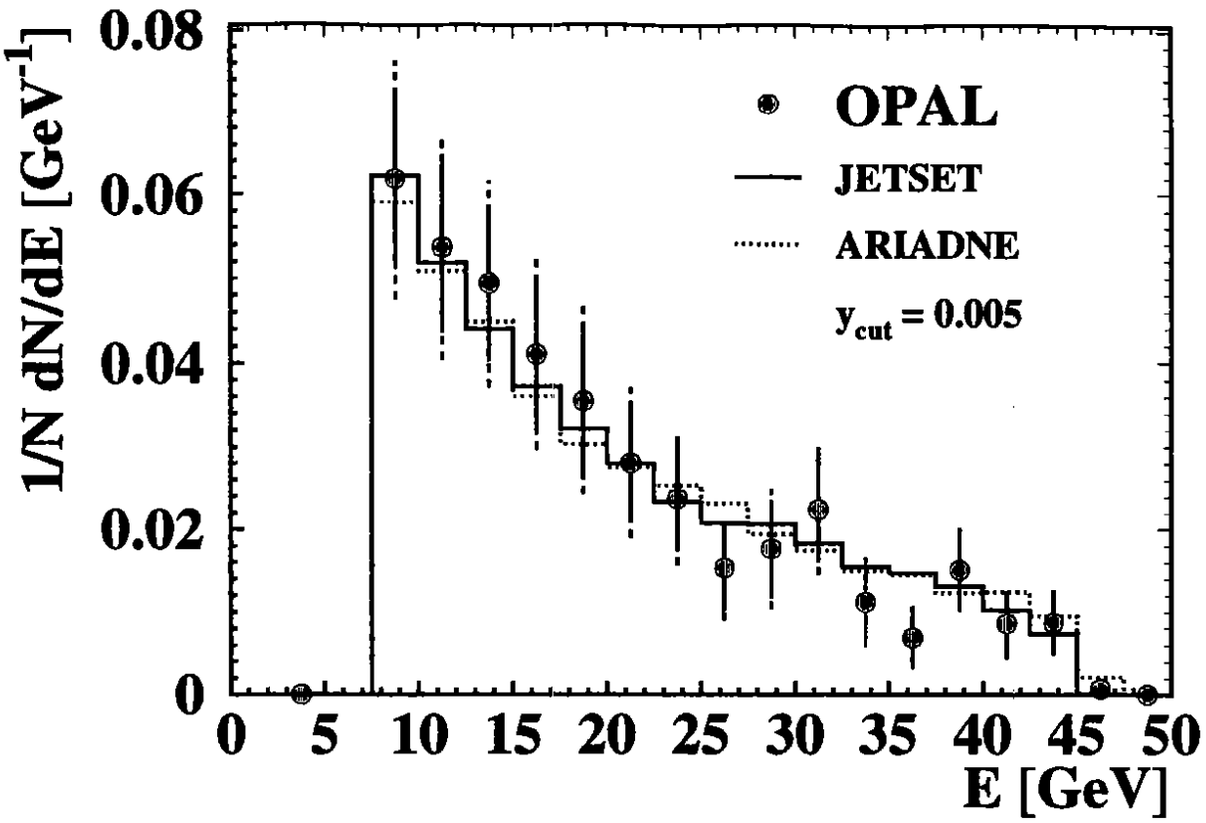
1/N dN/dE [GeV^{-1}]
0.08
0.06
0.04
0.02
0
OPAL
JETSET
ARIADNE
y_{cut} = 0.005
0 5 10 15 20 25 30 35 40 45 50
E [GeV]

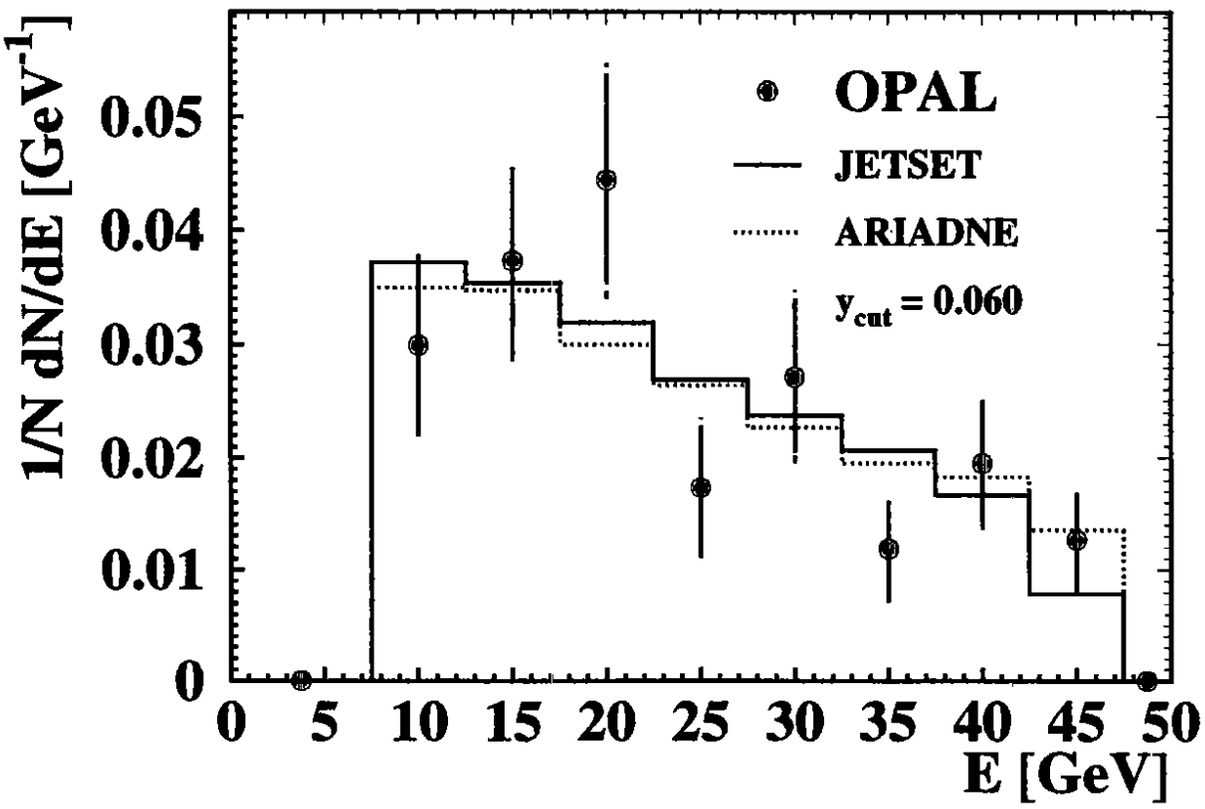
1/N dN/dE [GeV^{-1}]
0.05
0.04
0.03
0.02
0.01
0
OPAL
JETSET
ARIADNE
y_{cut} = 0.060
0 5 10 15 20 25 30 35 40 45 50
E [GeV]

Figure 8 a, b

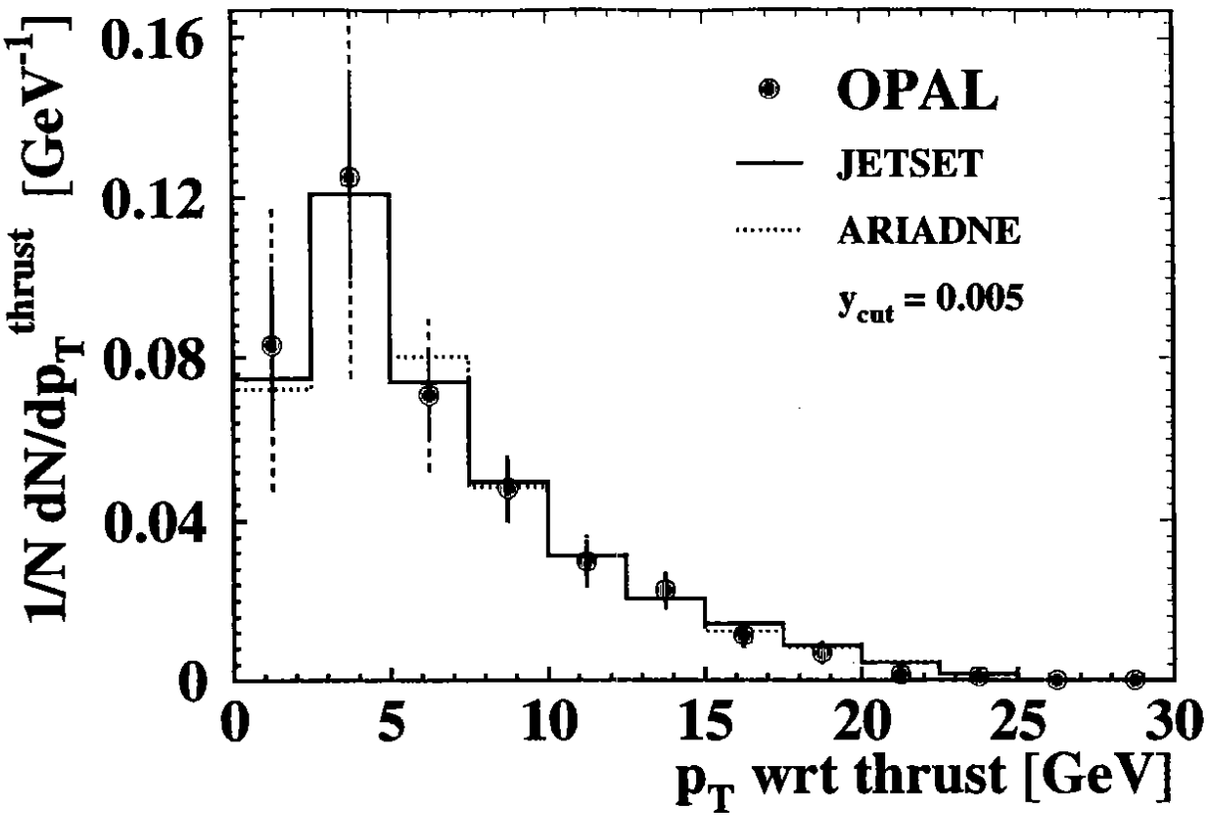
OPAL
JETSET
ARIADNE
y_{cut} = 0.005
$1/N\ dN/dp_T^{thrust}$ [GeV^{-1}]
p_T wrt thrust [GeV]
0.16
0.12
0.08
0.04
0
0
5
10
15
20
25
30

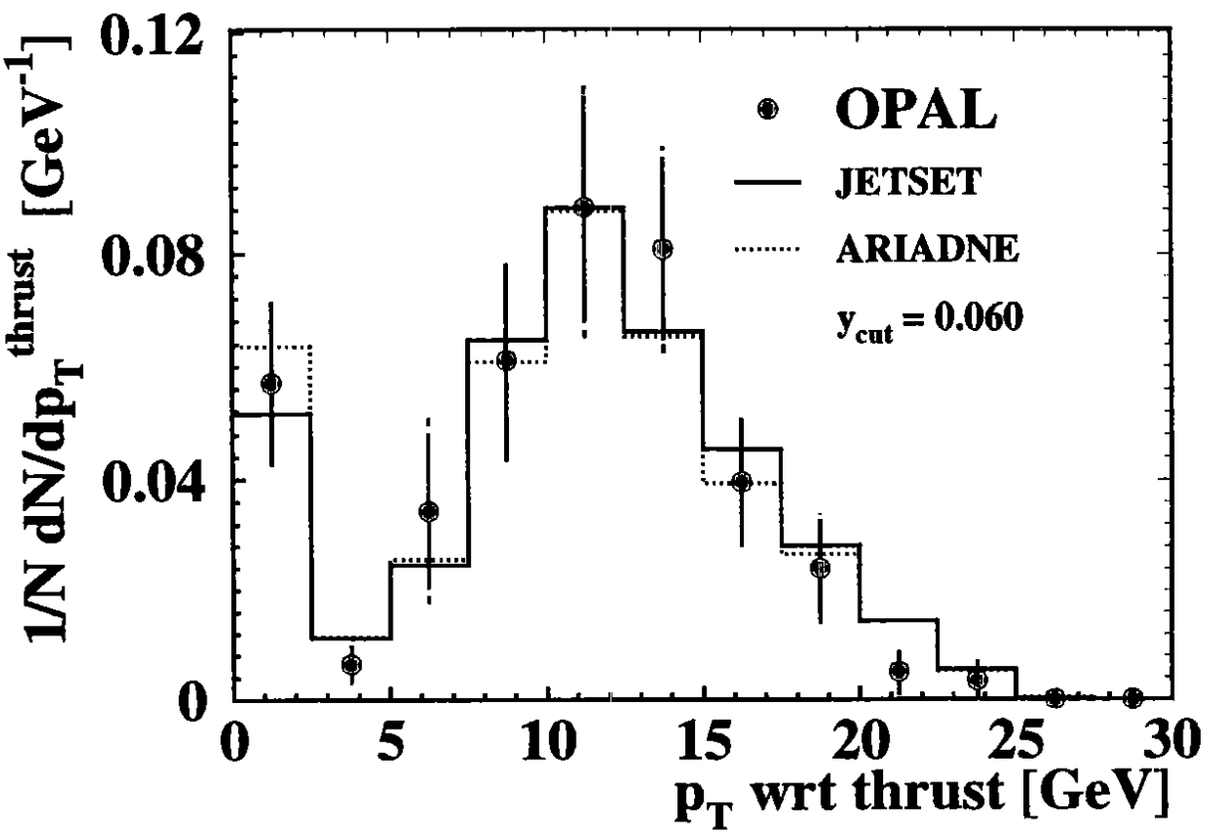
OPAL
JETSET
ARIADNE
y_{cut} = 0.060
$1/N\ dN/dp_T^{thrust}$ [GeV^{-1}]
p_T wrt thrust [GeV]
0.12
0.08
0.04
0
0
5
10
15
20
25
30

Figure 9 a, b

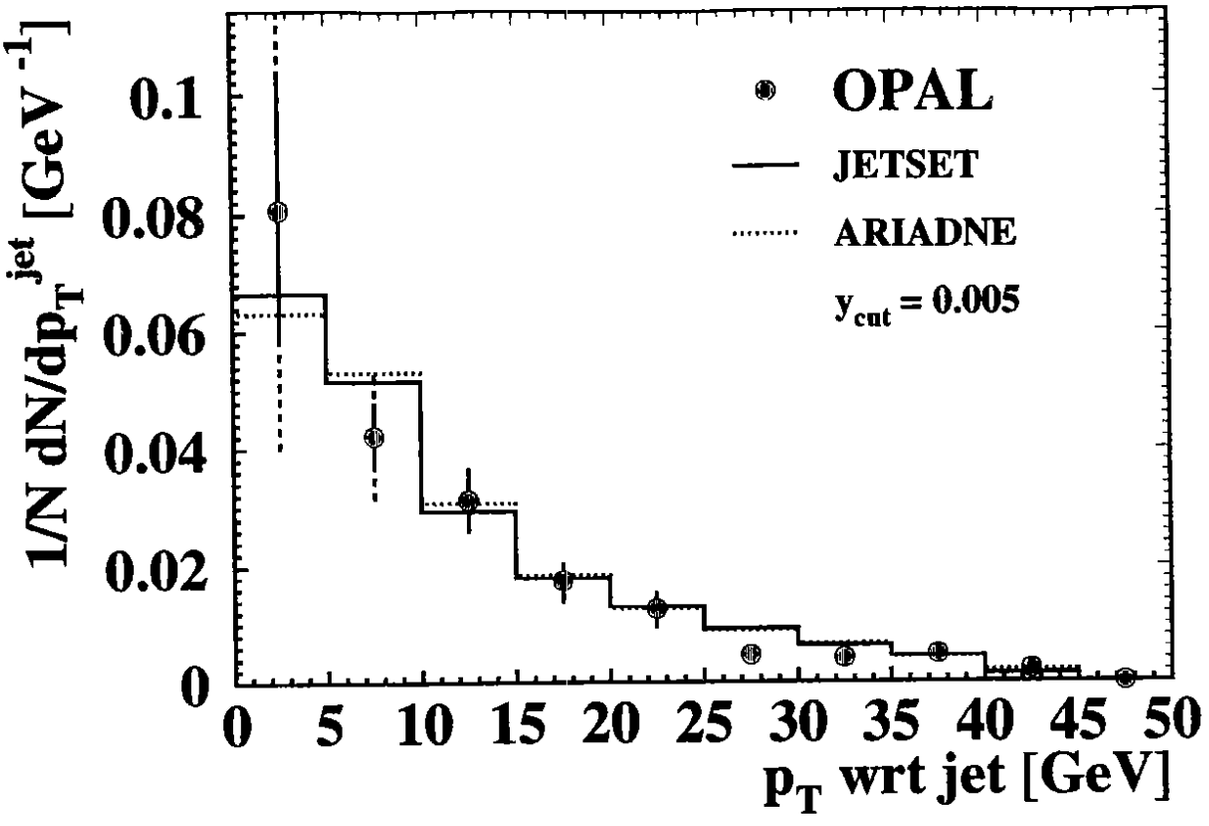
OPAL
JETSET
ARIADNE
y_{cut} = 0.005
$1/N\ dN/dp_T^{jet}$ [GeV^{-1}]
p_T wrt jet [GeV]
0
0.02
0.04
0.06
0.08
0.1
0 5 10 15 20 25 30 35 40 45 50

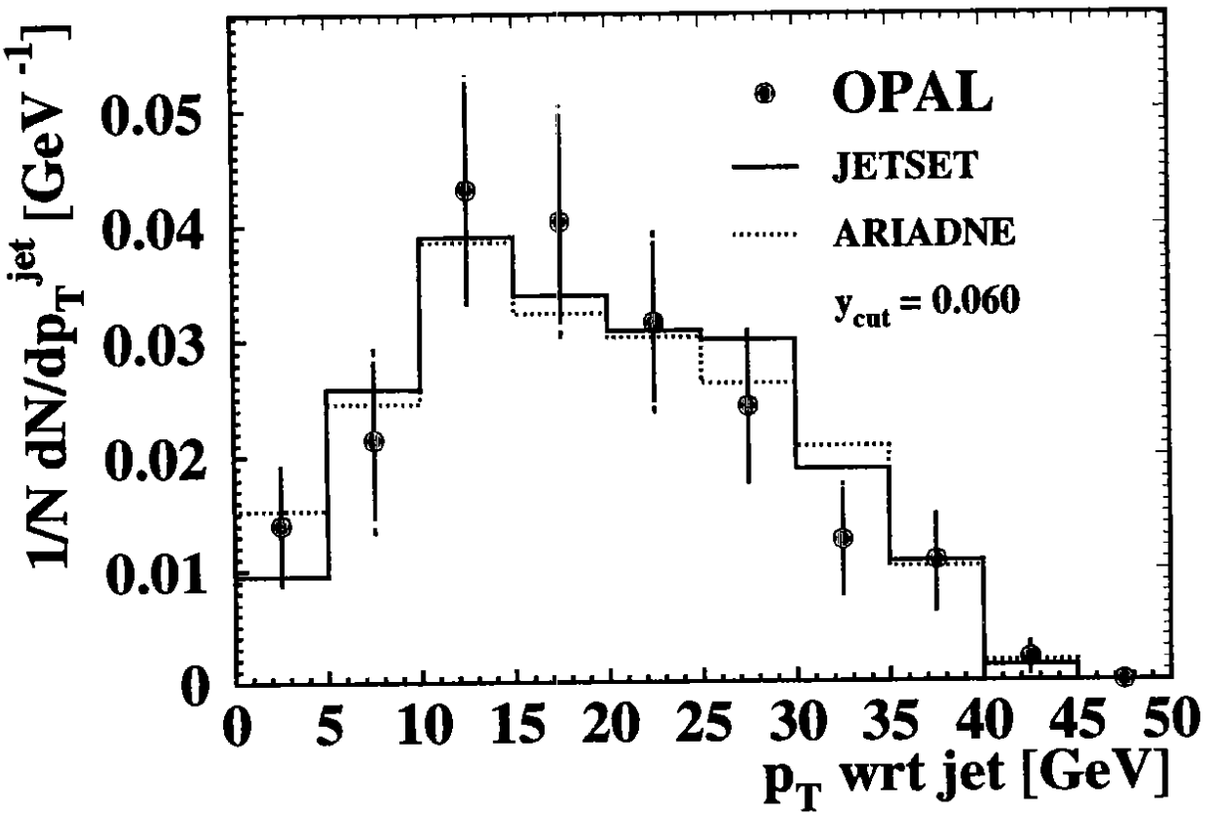
OPAL
JETSET
ARIADNE
y_{cut} = 0.060
$1/N\ dN/dp_T^{jet}$ [GeV^{-1}]
p_T wrt jet [GeV]
0
0.01
0.02
0.03
0.04
0.05
0 5 10 15 20 25 30 35 40 45 50

Figure 10 a, b

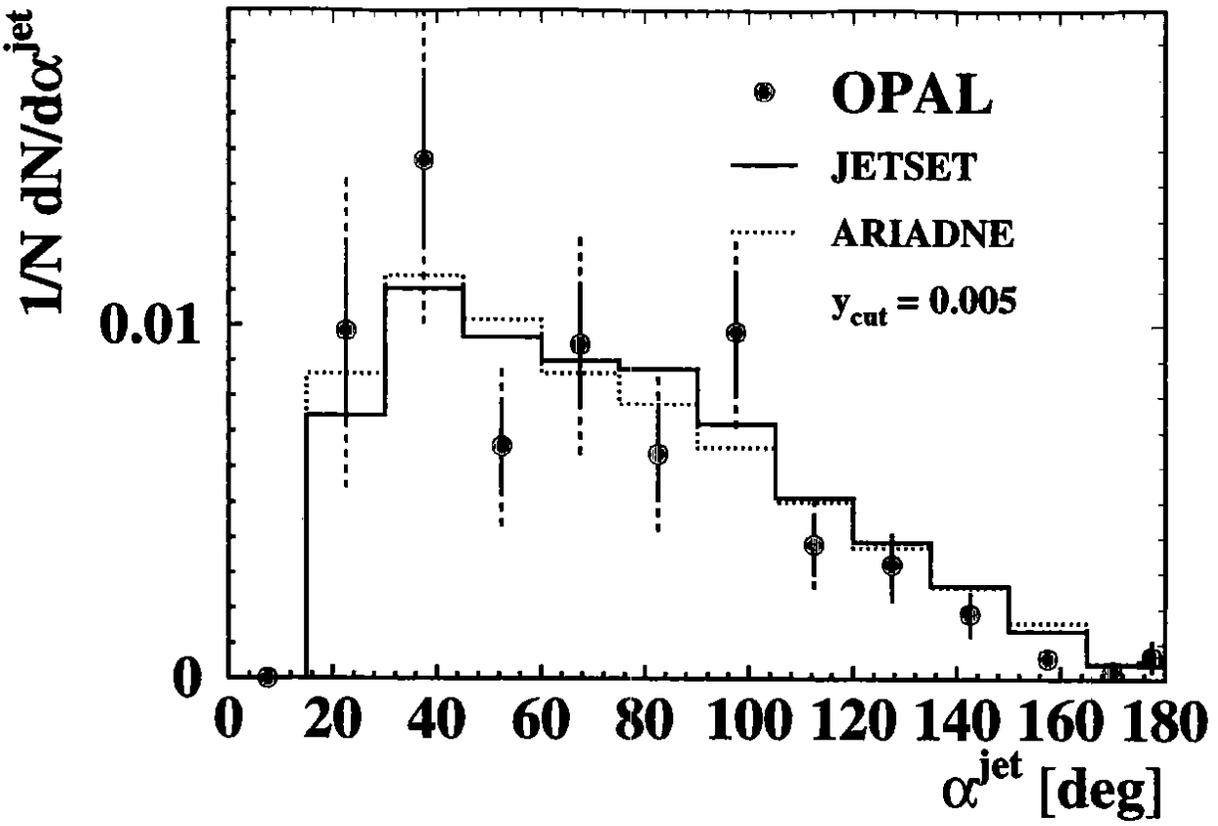
1/N dN/dα^jet
0.01
0
OPAL
JETSET
ARIADNE
y_cut = 0.005
0 20 40 60 80 100 120 140 160 180
α^jet [deg]

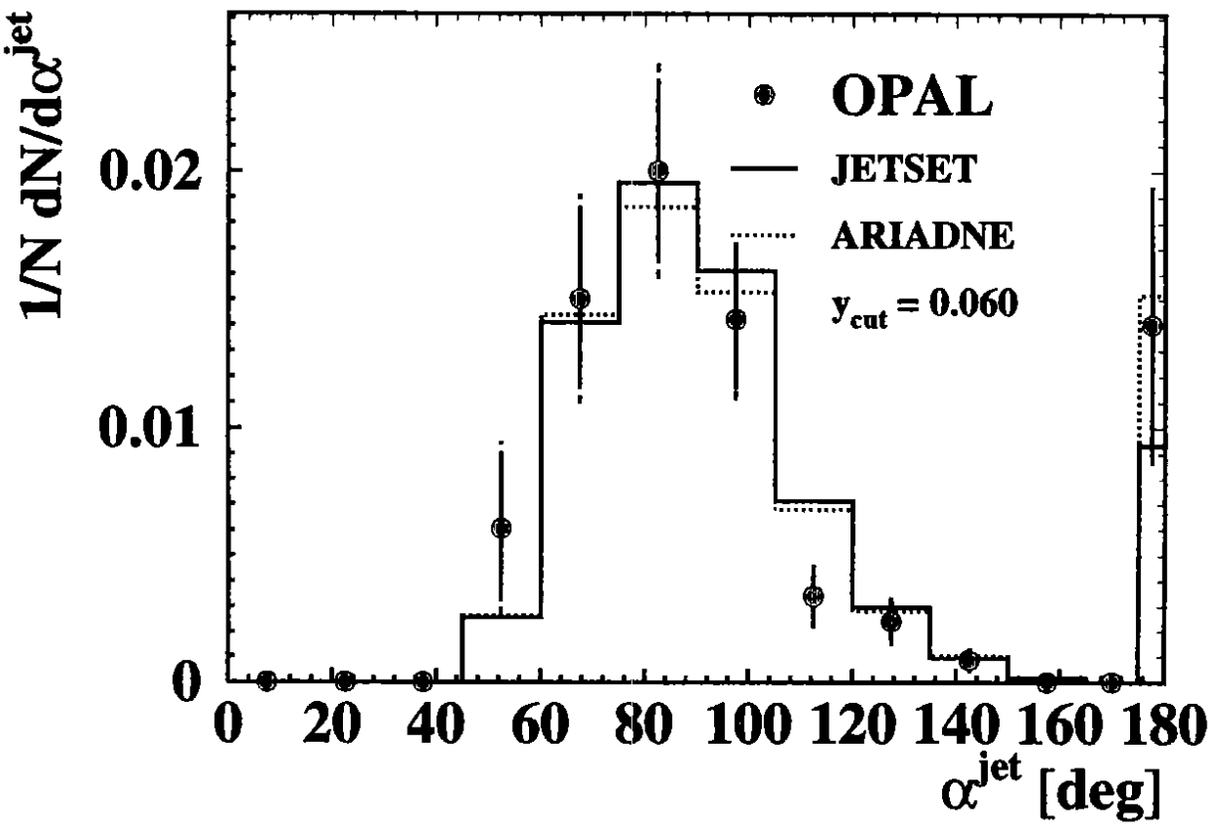
1/N dN/dα^jet
0.02
0.01
0
OPAL
JETSET
ARIADNE
y_cut = 0.060
0 20 40 60 80 100 120 140 160 180
α^jet [deg]

Figure 11 a, b

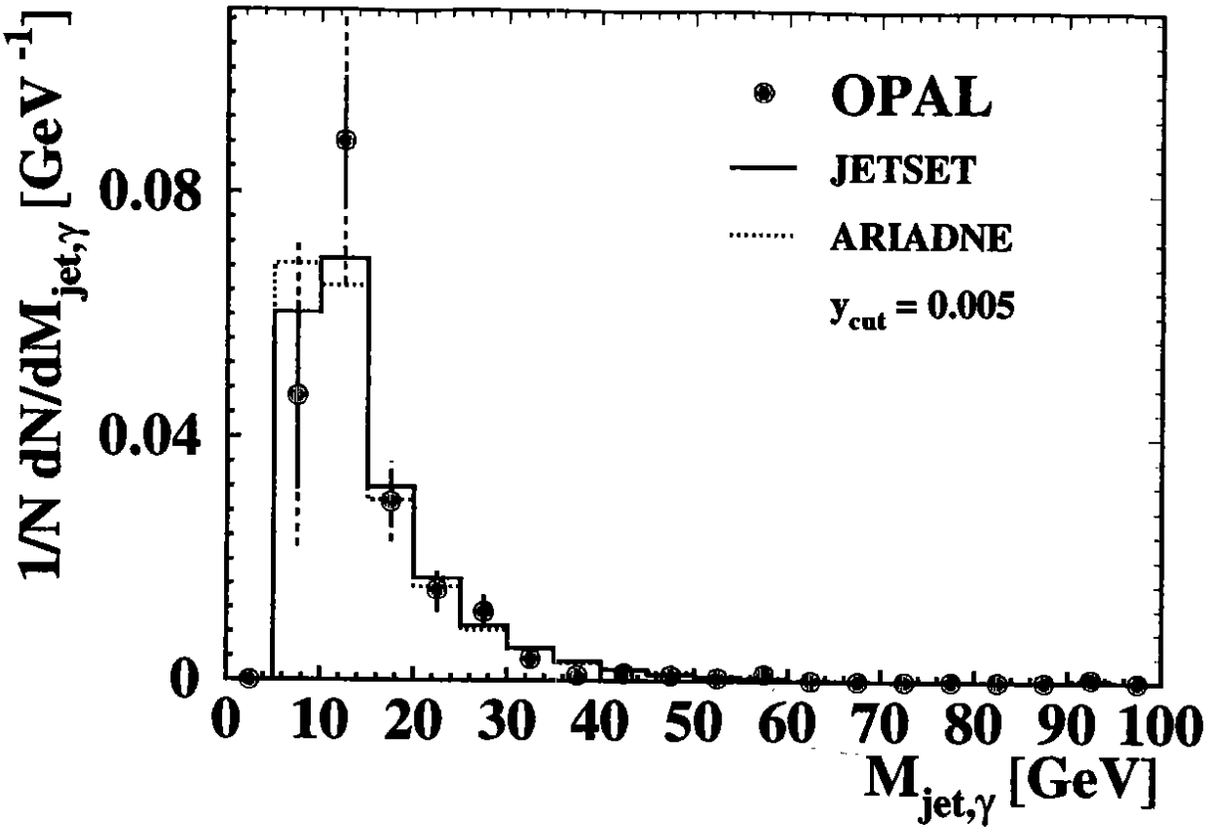
OPAL
JETSET
ARIADNE
y_{cut} = 0.005
1/N dN/dM$_{jet,\gamma}$ [GeV^{-1}]
0.08
0.04
0
0 10 20 30 40 50 60 70 80 90 100
M$_{jet,\gamma}$ [GeV]

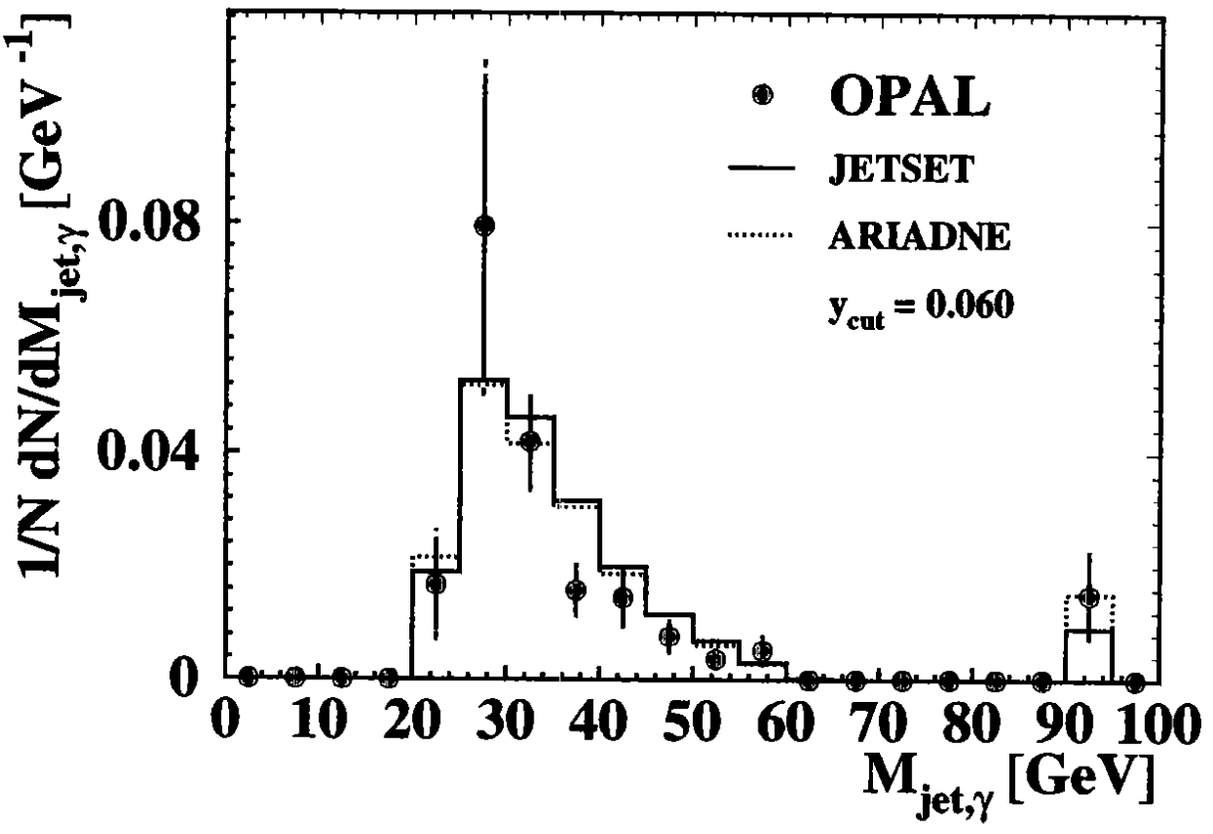
OPAL
JETSET
ARIADNE
y_{cut} = 0.060
1/N dN/dM$_{jet,\gamma}$ [GeV^{-1}]
0.08
0.04
0
0 10 20 30 40 50 60 70 80 90 100
M$_{jet,\gamma}$ [GeV]

Figure 12 a, b

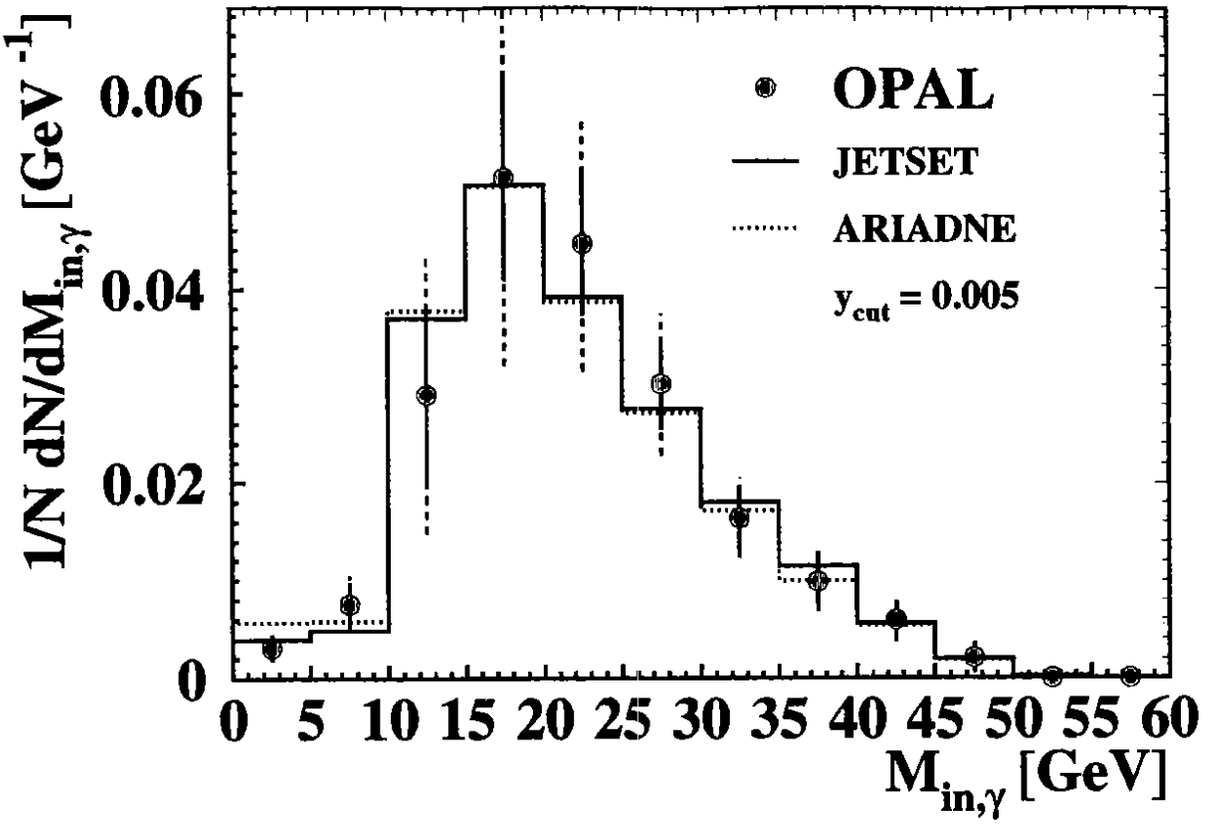
OPAL
JETSET
ARIADNE
y_{cut} = 0.005
1/N dN/dM$_{in,\gamma}$ [GeV^{-1}]
M$_{in,\gamma}$ [GeV]
0
0.02
0.04
0.06
0 5 10 15 20 25 30 35 40 45 50 55 60

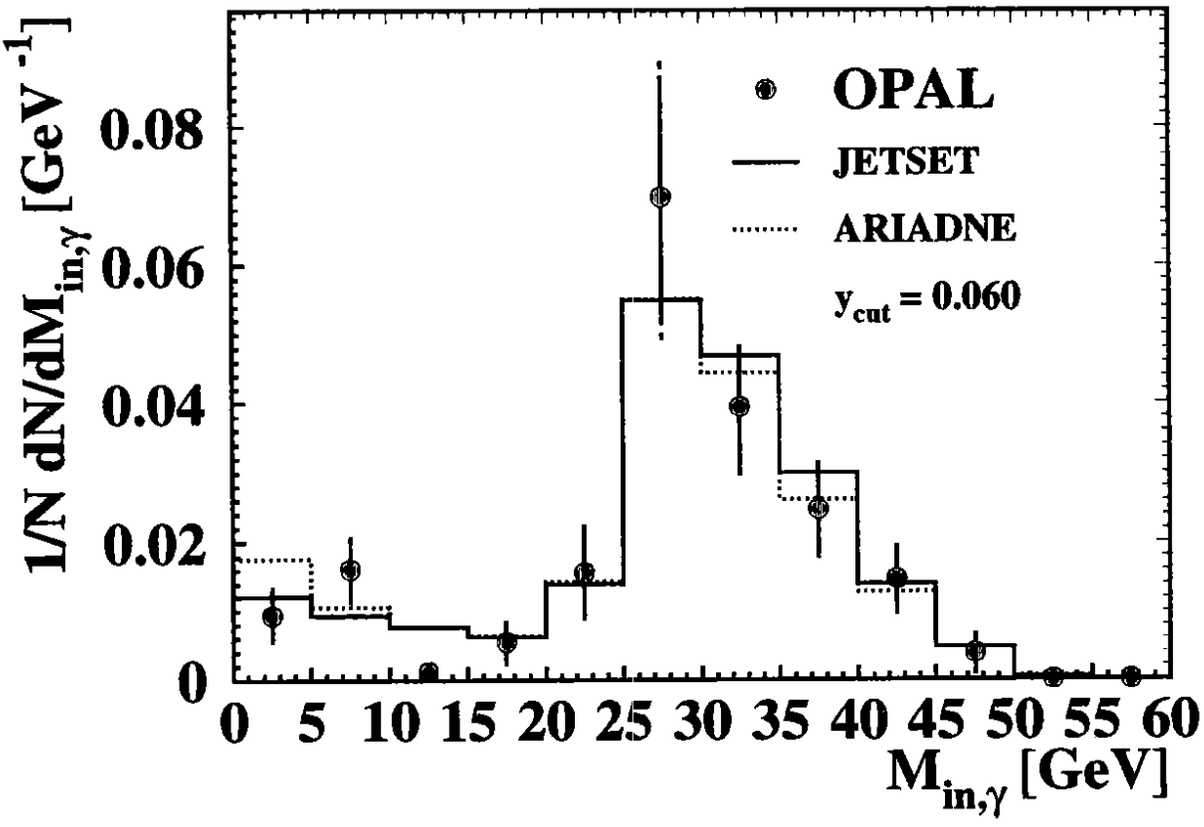
OPAL
JETSET
ARIADNE
y_{cut} = 0.060
1/N dN/dM$_{in,\gamma}$ [GeV^{-1}]
M$_{in,\gamma}$ [GeV]
0
0.02
0.04
0.06
0.08
0 5 10 15 20 25 30 35 40 45 50 55 60

Figure 13 a, b

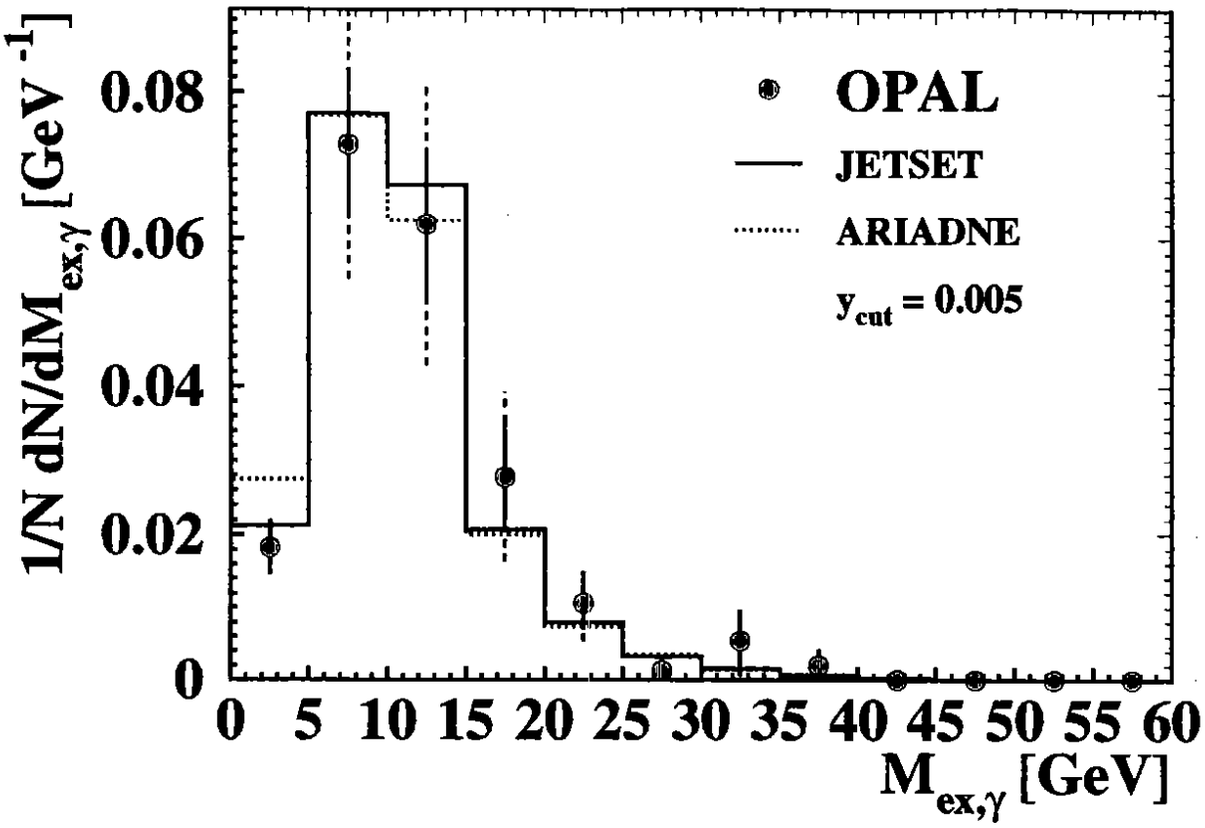
OPAL
JETSET
ARIADNE
y_{cut} = 0.005
1/N dN/dM$_{ex,\gamma}$ [GeV^{-1}]
0.08
0.06
0.04
0.02
0
0 5 10 15 20 25 30 35 40 45 50 55 60
M$_{ex,\gamma}$ [GeV]

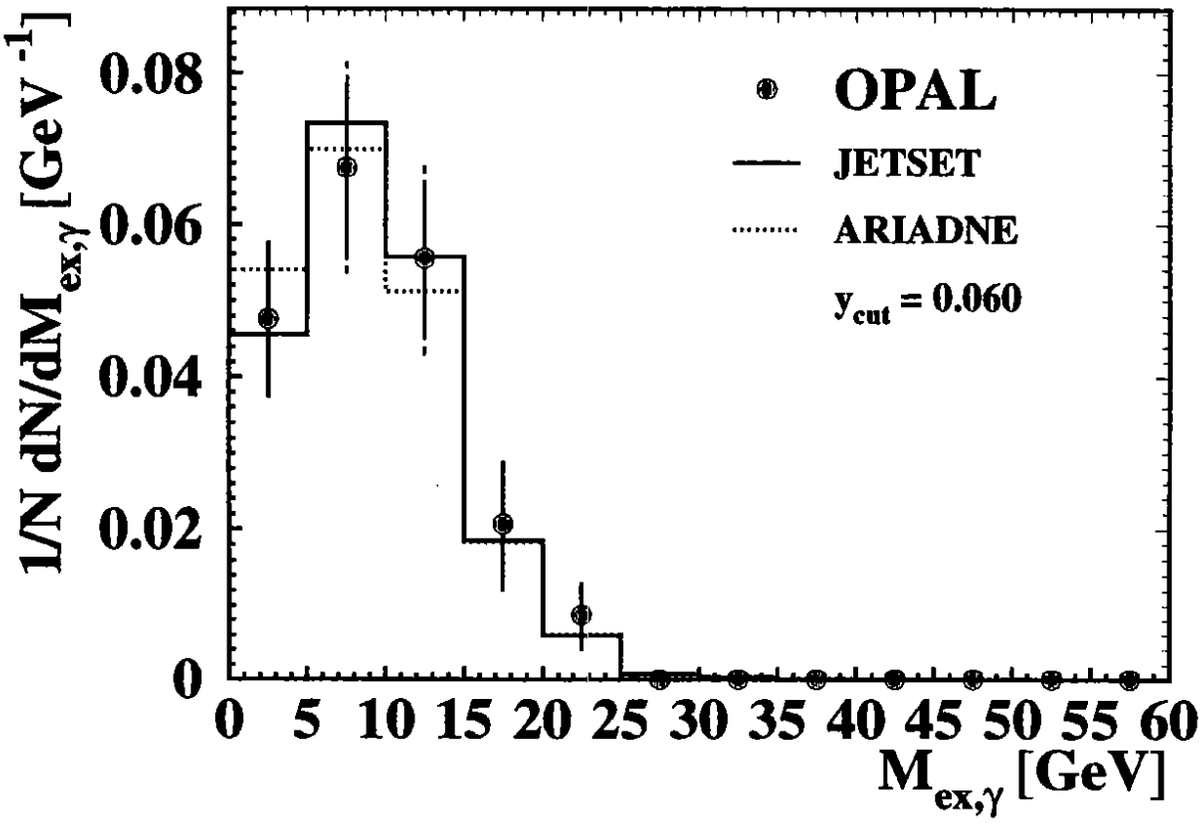
OPAL
JETSET
ARIADNE
y_{cut} = 0.060
1/N dN/dM$_{ex,\gamma}$ [GeV^{-1}]
0.08
0.06
0.04
0.02
0
0 5 10 15 20 25 30 35 40 45 50 55 60
M$_{ex,\gamma}$ [GeV]

Figure 14 a, b

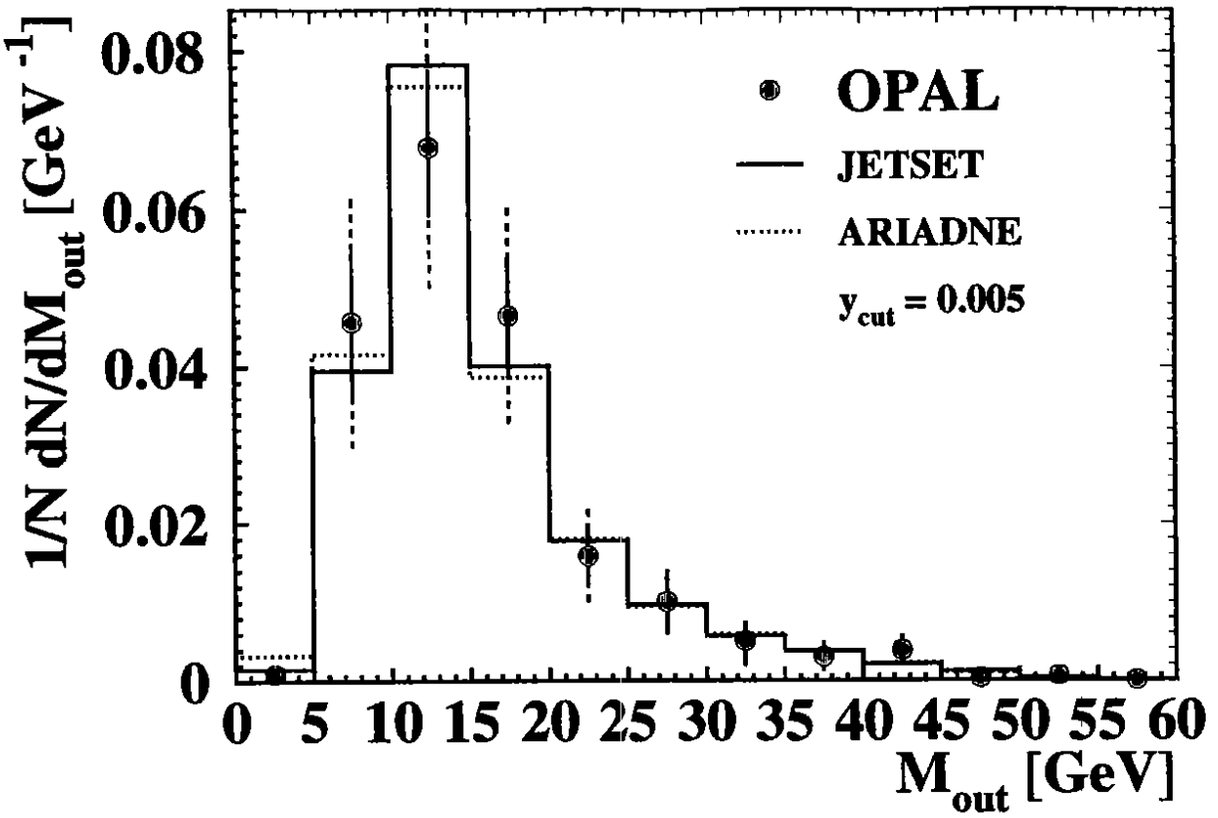

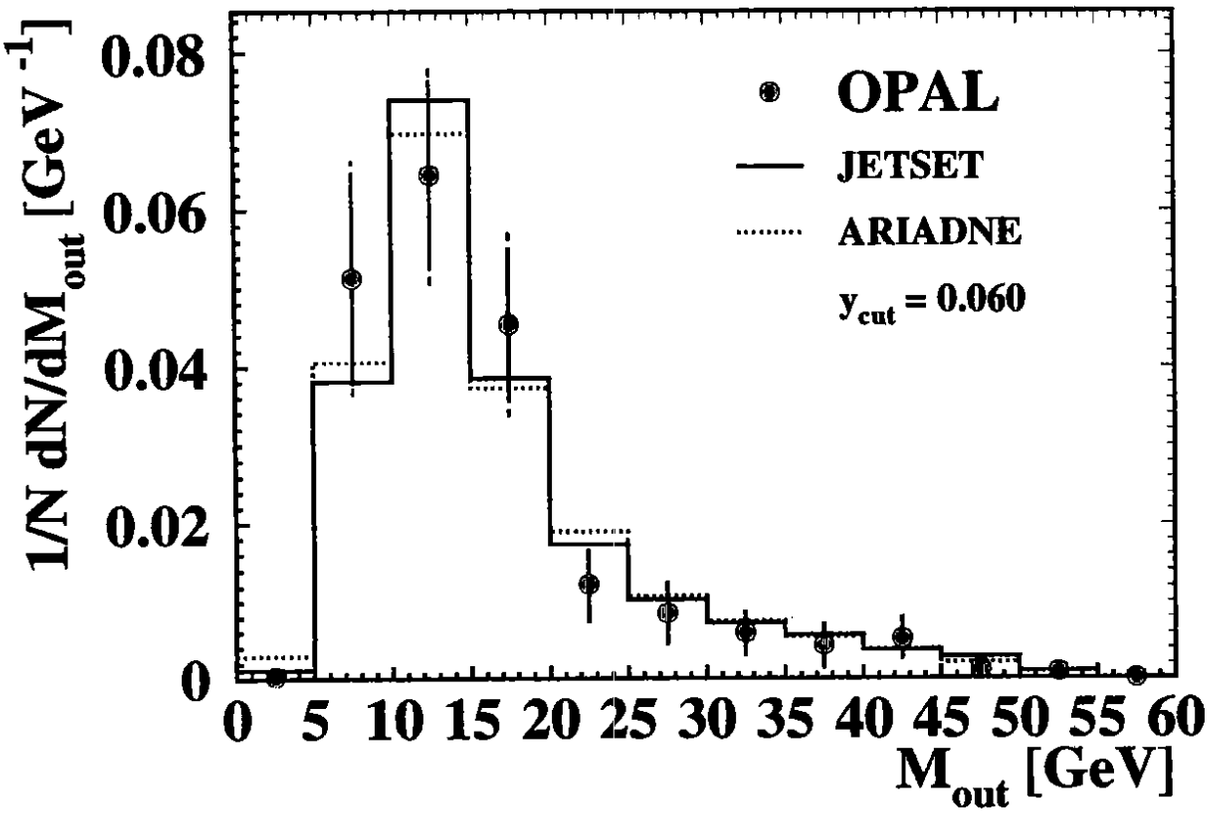

Figure 15 a, b

Imprimé au CERN. Prix : 1.25 Fr.